Cell Reports

Article

Proteomic screen reveals diverse protein transport between connected neurons in the visual system

Graphical abstract

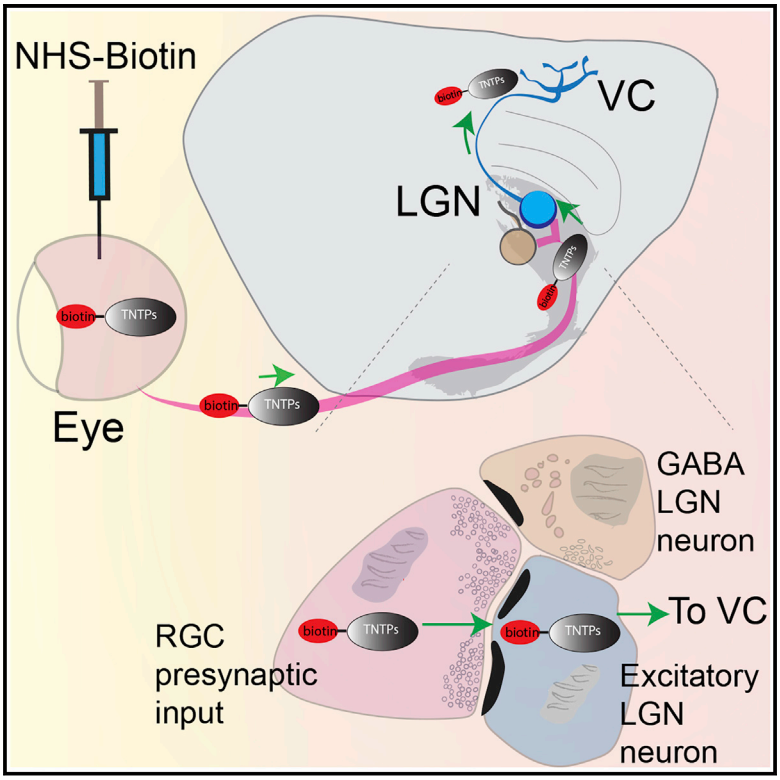

Highlights

- Mass spectrometry identifies ~200 proteins transported between neurons in the visual pathway
- Transneuronally transported proteins (TNTPs) include synaptic and axonal proteins
- TNTPs selectively transfer to excitatory but not inhibitory neurons
- Exosomes are involved in TNTP transport in the visual system

Authors

Lucio M. Schiapparelli, Pranav Sharma, Hai-Yan He, ..., Jeffrey L. Goldberg, John R. Yates III, Hollis T. Cline

Correspondence

cline@scripps.edu

In brief

Schiapparelli et al. show that diverse endogenous proteins are transported anterogradely across synapses in the rat visual system. About 200 transneuronally transported proteins (TNTPs) were identified by MS/MS, and selected TNTPs, including β-synuclein and tau, were validated using biochemical and histological methods. TNTP transport may be mediated by exosomes.

Schiapparelli et al., 2022, Cell Reports *38*, 110287
January 25, 2022
https://doi.org/10.1016/j.celrep.2021.110287

CellPress

Cell Reports

CellPress
OPEN ACCESS

Article

Proteomic screen reveals diverse protein transport between connected neurons in the visual system

Lucio M. Schiapparelli,[1,6] Pranav Sharma,[1,5] Hai-Yan He,[1,7,11] Jianli Li,[1,8,11] Sahil H. Shah,[1,2,3] Daniel B. McClatchy,[4] Yuanhui Ma,[4,9] Han-Hsuan Liu,[1,10] Jeffrey L. Goldberg,[3] John R. Yates III,[4] and Hollis T. Cline[1,12,*]

[1]Neuroscience Department and Dorris Neuroscience Center, The Scripps Research Institute, La Jolla, CA 92037, USA
[2]Neuroscience Graduate Program and Medical Scientist Training Program, University of California, San Diego, La Jolla, CA 92093, USA
[3]Byers Eye Institute and Spencer Center for Vision Research, Stanford University, Palo Alto, CA 94303, USA
[4]Department of Molecular Medicine, The Scripps Research Institute, La Jolla, CA 92037, USA
[5]Xosomix, 3210 Merryfield Row, San Diego, CA 92121, USA
[6]Present address: The Department of Cell Biology, Duke University Medical School, Durham, NC 27710, USA
[7]Present address: Department of Biology, Georgetown University, Washington, DC, USA
[8]Present address: Baylor Genetics, Houston, TX, USA
[9]Present address: Takeda Development Center Americas, Inc., San Diego, CA 92121, USA
[10]Present address: Howard Hughes Medical Institute, Department of Physiology, University of California, San Francisco, CA, USA
[11]These authors contributed equally
[12]Lead contact
*Correspondence: cline@scripps.edu
https://doi.org/10.1016/j.celrep.2021.110287

SUMMARY

Intercellular transfer of toxic proteins between neurons is thought to contribute to neurodegenerative disease, but whether direct interneuronal protein transfer occurs in the healthy brain is not clear. To assess the prevalence and identity of transferred proteins and the cellular specificity of transfer, we biotinylated retinal ganglion cell proteins *in vivo* and examined biotinylated proteins transported through the rodent visual circuit using microscopy, biochemistry, and mass spectrometry. Electron microscopy demonstrated preferential transfer of biotinylated proteins from retinogeniculate inputs to excitatory lateral geniculate nucleus (LGN) neurons compared with GABAergic neurons. An unbiased mass spectrometry-based screen identified ~200 trans-neuronally transported proteins (TNTPs) isolated from the visual cortex. The majority of TNTPs are present in neuronal exosomes, and virally expressed TNTPs, including tau and β-synuclein, were detected in isolated exosomes and postsynaptic neurons. Our data demonstrate transfer of diverse endogenous proteins between neurons in the healthy intact brain and suggest that TNTP transport may be mediated by exosomes.

INTRODUCTION

Intercellular interactions control diverse physiological processes in the brain, including cell and tissue development, neuro-immune responses, and synaptic plasticity. Identifying the mechanisms underlying these interactions may inform the biological processes they affect and increase our understanding of cellular interactions. One mode of intercellular communication that may occur in the brain is transfer of proteins between cells. Interneuronal transfer of toxic forms of tau and α-synuclein is thought to contribute to neuropathology in neurodegenerative diseases (Braak et al., 2003; Elfarrash et al., 2019; Hansen and Li, 2012; Kara et al., 2018), whereas interneuronal transfer of proteins such as brain-derived neurotrophic factor (BDNF) and orthodenticle homeobox 2 (OTX2) (Altar et al., 1997; Spatazza et al., 2013; Sugiyama et al., 2008) may affect brain development and plasticity. Whether and to what extent proteins transfer between neurons in the healthy adult brain is unknown. Classical studies in which intravitreal injections of radiolabeled amino acids labeled visual system connections (Bickford et al., 2010; Grafstein, 1971; Grafstein and Laureno, 1973; Reinis and Goldman, 1984; Rhodes and Gonatas, 1986; Specht and Grafstein, 1973), including the well-known ocular dominance columns (Wiesel et al., 1974), suggested that endogenous proteins are transported between synaptically connected neurons. Indeed, recovery of radiolabeled proteins from the visual cortex and analysis of their transport in the optic nerve (Grafstein and Forman, 1980) suggested that the amino acids were incorporated into proteins during *de novo* protein synthesis and transported anterogradely to connected neurons in the visual pathway. Nevertheless, it is still unclear whether intact proteins were transported between neurons in these experiments because of the possibility that radiolabeled proteins in retinal ganglion cells (RGCs) could be degraded, allowing radiolabeled degradation products to be transferred between neurons. Here we sought to

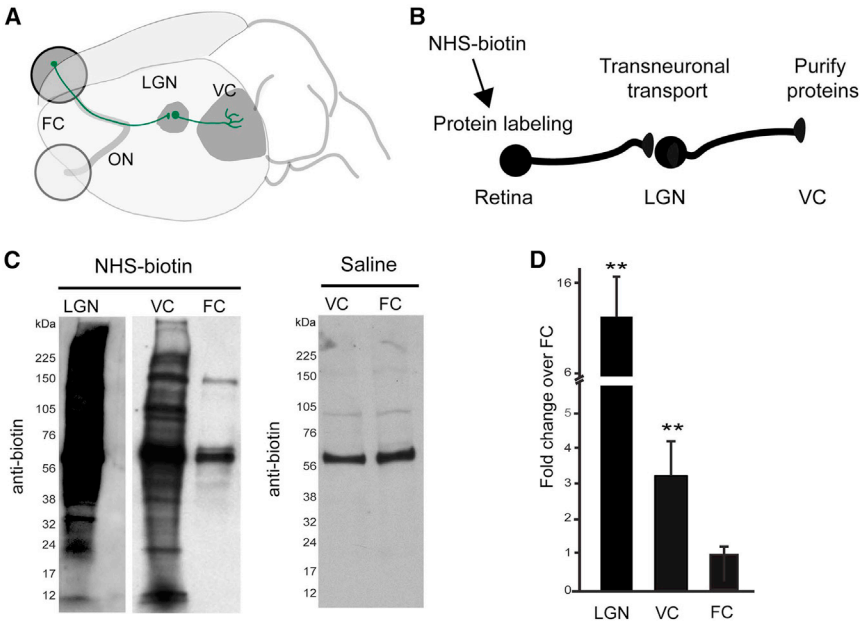

Figure 1. *In vivo* retinal protein biotinylation labels proteins in the VC

(A and B) Schematic of the rodent visual system and workflow to identify TNTPs.

(C) Western blots of biotin-labeled proteins from the lateral geniculate nucleus (LGN), visual cortex (VC), and frontal cortex (FC) after *in vivo* intravitreal injection of NHS-biotin or saline.

(D) Quantification of western blots, showing increased biotin-labeled proteins in the LGN and VC, normalized to the FC. n = 3 animals. Kruskal-Wallis test (ANOVA $p < 0.0001$) with Dunn's multiple comparison test; $^{**}p < 0.01$.

See also Figure S1.

conduct an unbiased screen to identify endogenous proteins that are transferred between neurons in the healthy intact brain and to visualize protein transfer as a means to understand the mechanism of intercellular protein transport.

We labeled proteins in the retina using *in vivo* intravitreal injections of *N*-hydroxy-succinimidobiotin (NHS-biotin) and used biochemistry, proteomics, and anatomical methods to analyze biotinylated proteins in the rodent visual system. NHS-biotin is a highly reactive protein labeling reagent that efficiently and covalently binds lysines and N-terminal amines of proteins, resulting in stable protein biotin labeling that cannot be reincorporated after protein degradation (Watanabe et al., 2007). Targeted retinal protein labeling with intravitreal NHS-biotin injection results in detection of biotinylated endogenous proteins specifically in retinorecipient visual areas (Schiapparelli et al., 2019). The visual system is composed of an anatomically distributed neuronal circuit in which presynaptic RGCs are spatially isolated from postsynaptic neurons in the thalamus, which, in turn, extend axons into the visual cortex (Paxinos and Watson, 1998). We reasoned that biotinylated proteins recovered from the visual cortex would have been transported from the retina via the optic tract, crossing at least one synapse in the lateral geniculate nucleus (LGN) to reach the visual cortex. Light and electron microscopy to detect biotin immunolabeling in RGC axon terminals and postsynaptic LGN neurons revealed preferential transfer to excitatory LGN neurons compared with GABAergic neurons. We conducted an unbiased proteomics screen to identify transneuronally transported proteins (TNTPs) in the adult rat visual system by combining *in vivo* protein biotin labeling, biochemical purification of biotinylated proteins from the visual cortex, and tandem mass spectrometry (MS/MS)-based identification of biotinylated peptides from labeled retinal proteins. Our MS/MS screen identified about 200 TNTPs, which are annotated to multiple functional categories and subcellular compartments, including exosomes. The majority of TNTPs were detected in neuronal exosome proteomes, suggesting that exosomes are a mechanism of intercellular TNTP transfer. Virally expressed TNTPs, including tau and β-synuclein fused to FLAG or cre recombinase, were detected in postsynaptic neurons and could drive reporter gene expression, suggesting that these findings may contribute to generation of new strategies for transsynaptic neuronal labeling. These data demonstrate that intact endogenous proteins are transferred between neurons in the healthy intact brain and that TNTPs fall into diverse categories and are distributed widely within target neurons, including distant axon projections.

RESULTS

In vivo intravitreal protein biotinylation labels proteins recovered from the visual cortex

We labeled retinal proteins by intravitreal injection of NHS-biotin and harvested tissue from the retina, LGN, visual cortex (VC), and frontal cortex (FC), a non-visual control area (Figures 1A and 1B). We observed biotinylated proteins over a range of molecular weights in western blots of the LGN and VC, whereas only endogenously biotinylated carboxylases (McKay et al., 2008) were seen in western blots of the FC and controls with intravitreal saline injections (Figures 1C and 1D), similar to results following intravitreal injection of radiolabeled amino acids (Figure S1). Light microscopy demonstrated strong biotin labeling in the optic tract and LGN, including in RGC presynaptic boutons (Figures 2A–2C). The presence of biotinylated proteins in western blots of the VC suggested that proteins were transported from presynaptic RGC terminals to dendrites of LGN relay neurons and then routed through LGN neuronal somata to geniculocortical axons in the VC. Indeed, following monocular intravitreal NHS-biotin injection, the biotin label was detected in neuronal somata in the innervated region of the contralateral LGN by light and immunoelectron microscopy but not in corresponding regions of the ipsilateral LGN (Figure S2).

Ultrastructural visualization of transneuronal protein transport at retinogeniculate synapses reveals preferential transfer to glutamatergic LGN neurons

We analyzed retinogeniculate inputs as the source of transneuronal protein transport at the ultrastructural level and

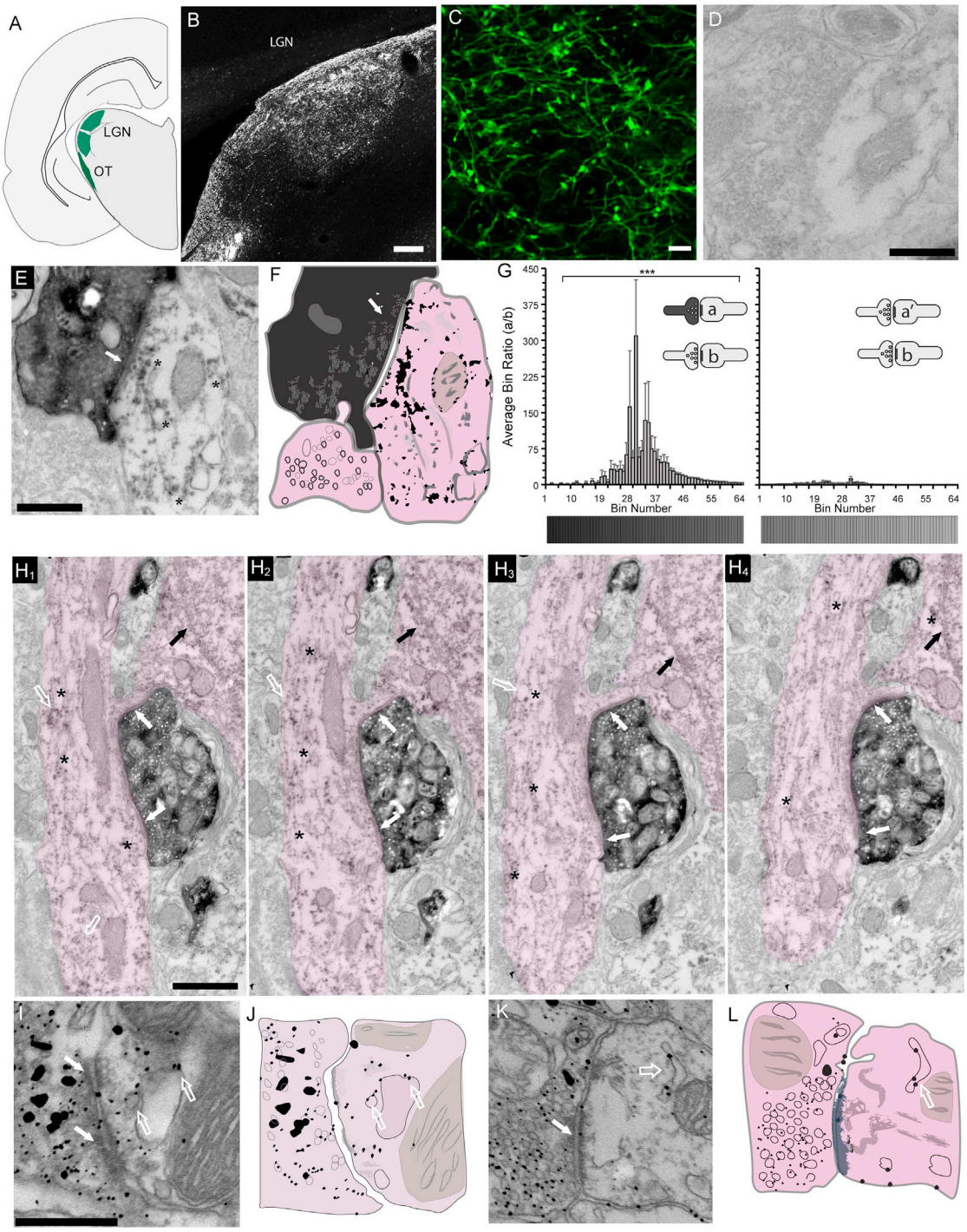

Figure 2. Ultrastructural detection of postsynaptic transneuronal biotin-labeled proteins in the LGN

(A) Drawing of a coronal brain section showing the optic tract (OT) and LGN.

(B) Single confocal optical section through the LGN contralateral to the NHS-biotin-injected eye, showing transported biotinylated proteins in RGC axons. Scale bar, 50 μm.

(C) RGC axons and presynaptic boutons in the LGN, visualized by immunolabeling transported biotinylated proteins. Scale bar, 10 μm.

(D and E) Immuno-EM images of control unlabeled (D) and NHS-biotin protein-labeled (E) retinogeniculate synapses from the same section. (E) shows dense biotin label in the presynaptic RGC axon terminal and filamentous biotin label in the postsynaptic LGN dendrite (black asterisks). The white arrow highlights the retinogeniculate synapse. Scale bars, 0.5 μm.

(legend continued on next page)

examined postsynaptic profiles for biotin immunoelectron microscopy (immuno-EM) labeling. We identified retinogeniculate synapses based on the presence of presynaptic vesicles in biotin+ terminals, a uniform synaptic cleft, and a postsynaptic density in the postsynaptic profile. We then scored the presence of biotin immunolabeling in the postsynaptic profile in that section and in neighboring serial sections. Examining serial EM sections increased confidence in identification of the biotin immunolabel in postsynaptic sites. EM of retinogeniculate synapses shows dense biotin labeling in presynaptic RGC axon terminals and the biotin label in postsynaptic dendrites of LGN neurons (Figures 2E and 2F) that can be readily distinguished from unlabeled profiles from the same material (Figure 2D). Quantification shows that biotin transfer is increased significantly in postsynaptic profiles apposed to labeled versus unlabeled presynaptic sites (Figure 2G).

Biotin labeling in postsynaptic profiles extended through dendritic processes, highlighting a filamentous meshwork seen across serial sections (Figures 2E, 2H$_{1-4}$, S3A$_{1-4}$, and S3B$_{1-2}$). In Figure 2H, the labeled dendrite extends from the cell body, where biotin labeling is also detected. Biotin labeling can also be seen in the dendritic profile adjacent to the biotin-labeled RGC axon in the lower right of the series of images. Immuno-EM biotin detection with streptavidin-FluoroNanogold revealed biotin labeling associated with membrane compartments in postsynaptic profiles (Figures 2I–2L, white hollow arrows) that resemble endosomes and tubular recycling endosomes (Harris and Weinberg, 2012). Similar biotin labeling associated with endocytic compartments is marked by white hollow arrows in Figure 2H$_{1-4}$.

Postsynaptic profiles with biotin immunolabeling were often adjacent to or in the same sections as postsynaptic profiles with no biotin immunolabeling (Figures 2E and S4A–S4D), suggesting possible regulated transfer to some postsynaptic sites but not others. In addition to terminating on glutamatergic geniculocortical relay neurons, RGCs synapse on dendrites of local GABAergic neurons, called F2 profiles (Figures 3A and S4), which, in turn, synapse on glutamatergic relay neurons in the well-described triad synapse (Erisir et al., 1998; Li et al., 2003; Sherman, 2004). The GABAergic profiles in the LGN triad synapse can be identified by distinctive ultrastructural morphological features: they are postsynaptic to retinal inputs, presynaptic to dendrites of LGN neurons, and filled with loosely packed synaptic vesicles. Based on these morphological criteria, postsynaptic profiles without the biotin label appeared to be GABAergic F2 profiles, suggesting that interneuronal transfer of NHS-biotin-labeled proteins to excitatory neurons occurs selectively.

To address this quantitatively, we collected serial ultrathin sections and analyzed retinogeniculate synapses to identify sites with and without biotinylated protein transfer into postsynaptic sites (Figures 3B–3E). We used post-embedding immunogold labeling with GABA antibodies (Li et al., 2003) in a subset of the sections (Figure 3B$_{1-3}$) to confirm that the profiles identified by morphological criteria are GABAergic. About one-third of retinogeniculate synapses terminate onto GABAergic F2 profiles (Figures 3F, total, and 3G, no transfer), consistent with previous studies (Beaulieu and Cynader, 1992; Montero and Singer, 1985). Of 210 retinogeniculate synapses with biotin-labeled presynaptic terminals, we detected biotin in the postsynaptic profile of 114 synapses (54%). 94% of the biotin-labeled postsynaptic profiles were glutamatergic geniculocortical relay cells, and 6% were GABAergic F2 profiles (Figures 3F, biotin+, and 3G, transfer). This distribution is significantly different ($p < 0.05$, Fisher's exact test) from the distribution of retinogeniculate synapses onto glutamatergic and GABAergic F2 profiles (65% and 35%, respectively) (Figures 3F, total, and 3G no transfer; Table S1). These data show that interneuronal protein transport at retinogeniculate synapses occurs preferentially to excitatory LGN neurons (Figure 3H), indicating that transfer is a regulated process targeting specific neuron types.

TNTPs from the VC are synaptic and axonal proteins present in neuronal exosomes

We applied MS/MS to identify biotinylated TNTPs labeled in the retina and recovered from the VC, identifying 210 TNTPs from 7 independent MS/MS experiments (Figures S5A–S5C; Table S3). In each experiment, 10–12 animals received intravitreal injections of NHS-biotin or saline, and tissue was collected after 11 days from the 2 treatment groups. Protein samples were processed for MS/MS using 2 independent strategies (Figure S5A): direct detection of biotin-containing tags (DiDBiT), 2 experiments) and Neutravidin protein enrichment (5 experiments). The DiDBiT strategy identified 127 biotinylated TNTPs, and the NeutrAvidin protein enrichment strategy identified 119 TNTPs, 36 of which overlapped with the TNTPs identified by DiDBiT (Figures S5B and S5C; Table S3).

We tested whether biotin-tagged TNTPs were enriched in the VC compared with the FC using several biochemical strategies. First, western blots of NeutrAvidin pull-down showed that β-synuclein, Munc18, Ca^{2+}/calmodulin-dependent protein kinase II

(F) Schematic of synaptic structures in (E), showing the RGC presynaptic terminal (dark), the postsynaptic spine with biotin immunolabeling (pink with black), and an unlabeled synaptic profile with synaptic vesicles (pink).

(G) Quantification of biotin intensity in postsynaptic profiles opposite biotin-labeled presynaptic profiles (a in the schematic on the left) and control unlabeled synapses (a' in the schematic on the right). See also STAR Methods. The LUT for the intensity scale is shown under the x axis. Data are plotted as mean ± SEM of normalized pixel intensities. n = 8 synapses for labeled (left) and 10 synapses for unlabeled (right) from samples from 3 different animals. ***$p < 0.0001$, calculated by comparing histograms using two-way ANOVA with Sidak correction for multiple comparisons. See Figure S3 for data from each NHS-biotin-labeled and control image.

(H$_{1-4}$). Serial sections through a biotin-labeled retinogeniculate terminal with a synapse (white arrows) onto a dendrite (pink) that contains biotin immunolabeling associated with a filamentous network (black asterisks). Scale bar, 0.5 μm. The nuclear membrane of the neuronal cell body is identified by the black arrow. The dendrite adjacent to the biotin-labeled RGC axon profile in the lower right of the series of images also contains a biotin label.

(I–L) Biotinylated protein visualized with streptavidin-FluoroNanogold labeling is detected in presynaptic sites (left) and the postsynaptic profile (right) in EM images (I and K) and the corresponding schematics (J and L). Biotin labeling is associated with postsynaptic endocytic compartments (white hollow arrows in H–L). Scale bar in (I), 0.5 μm (also applies to J–L).

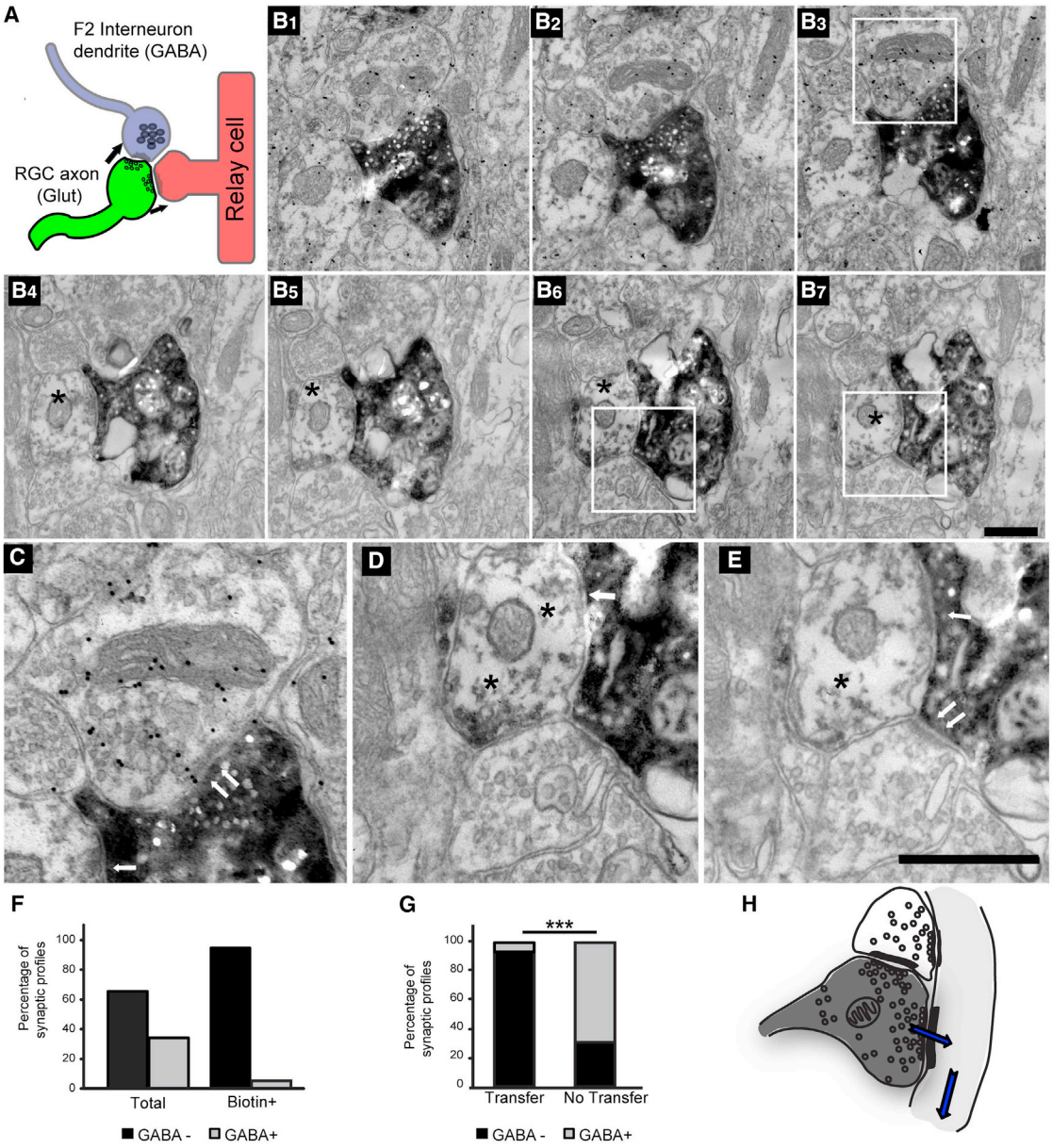

Figure 3. TNTPs are transported preferentially from retinal inputs to excitatory LGN neurons

(A) Schematic of the triad synapse in which RGC inputs (green) synapse onto geniculocortical relay cells (red) and vesicle-filled profiles from GABAergic neurons.

(B_{1-7}) Images of serial EM sections through a biotin-labeled retinogeniculate terminal contacting several postsynaptic dendrites. Biotin was visualized with horseradish peroxidase (HRP), and sections (B_{1-3}) were also labeled to visualize GABA immunoreactivity with 5-nm immunogold particles.

(C–E) Enlargements of boxed areas in ($B_{3,6,7}$). The postsynaptic profile, boxed in (B_3) and enlarged in (C), is a local GABAergic F2 terminal. The same biotin-labeled retinogeniculate input synapses on a GABA-negative dendrite (B_{1-7}), shown with a black asterisk boxed in ($B_{6,7}$) and enlarged in (D) and (E). The biotin immunolabel is detected in the GABA-negative profile (D and E), not in the GABA+ profile (C). Synapses are marked by white arrows.

Scale bars in (B) and (E), 0.5 μm. The scale bar in (E) also applies to (C) and (D)

(F and G) Quantification of the percentage of GABA+ and GABA− postsynaptic profiles with a biotin label.

(F) 94% of biotin-labeled postsynaptic profiles were GABA− versus the total distribution, in which 65% of postsynaptic profiles were GABA− (n = 114 synapses).

(G) Biotinylated protein transfer occurs preferentially from retinogeniculate terminals to postsynaptic GABA− profiles. ***$p < 0.001$ (Fisher's exact test).

(H) Drawing of a retinogeniculate triad synapse, showing selective protein transport to excitatory postsynaptic profiles.

(CaMKII), syntaxin 1A, tau, and synaptotagmin 1 were enriched in the VC compared with the FC (Figure 4A). Second, we detected biotinylated TNTPs in immuno-pull-down of Munc18, CaMKII, and syntaxin 1A from the VC but not the FC (Figure 4B) and not in the VC of saline-treated animals (Figure 4C). Third, by combining TNTP immuno-pull-down from the VC or FC followed

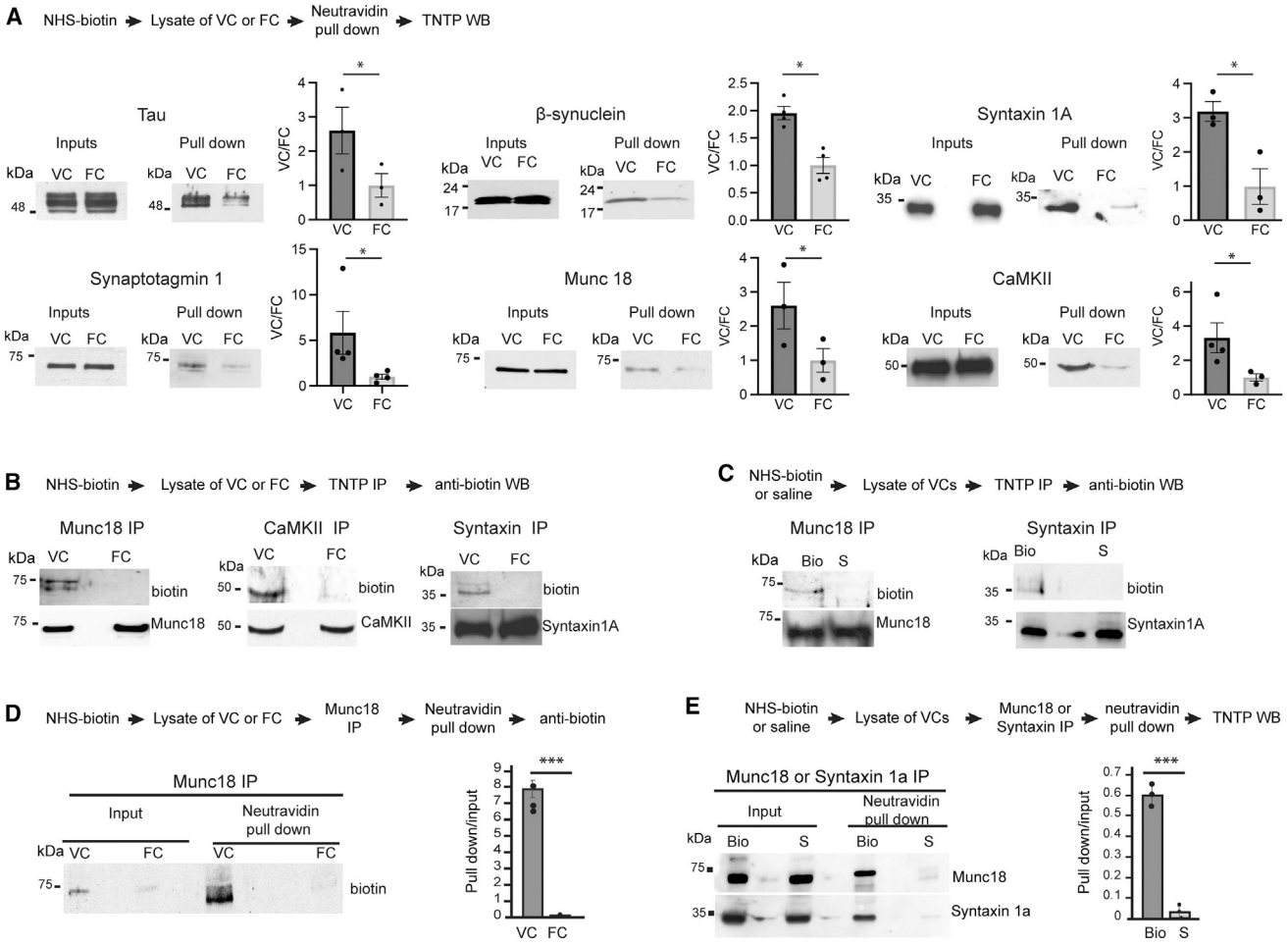

Figure 4. Detection of biotin-labeled TNTPs from the VC

The experimental workflow is shown at the top of each panel.

(A) NHS-biotin-labeled proteins from the VC or FC were purified by NeutrAvidin pull-down and probed on western blots for the TNTPs tau, β-synuclein, syntaxin 1A, synaptotagmin 1, Munc18, and CaMKII. Right: western blot analysis, as ratio of NeutrAvidin pull-down normalized to the input. n = 4.

(B) The TNTPs Munc18, CaMKII, and Syntaxin 1A were immunoprecipitated from the VC or FC. The anti-biotin antibody and the TNTP antibody detect biotinylated TNTP and total TNTP in the VC and FC, respectively.

(C) Biotinylated TNTPs were detected in the VC only after intravitreal NHS-biotin (Bio) but not saline (S) injection.

(D) Two-step purification of biotinylated Munc18 by immunoprecipitation (IP) with a Munc18 antibody, followed by NeutrAvidin pull-down, showed enrichment of biotinylated Munc18 in the VC. Right: quantification of the western blot.

(E) Two-step purification of TNTP IP, followed by NeutrAvidin pull-down, assayed with a TNTP western blot. Munc18 and Syntaxin 1A were enriched in the VC of animals that received Bio but not S. Right: quantification of the western blots.

For (B)–(E), n = 3 (*p < 0.05, ***p < 0.001, Welch's t test).

by NeutrAvidin pull-down, we detected biotinylated Munc18 and syntaxin 1A selectively in the VC (Figures 4D and 4E). Our histology, MS/MS, and biochemistry results indicate that endogenous proteins are transported between neurons in the visual system of rats.

MS/MS of biotinylated proteins from the VC allows unbiased analysis of proteins that are transported between neurons in the intact brain. 95% of TNTPs are annotated to synaptic sites, whereas about 60% are annotated to axons and extracellular vesicles (Figures 5B, 5F, S5D, and S5E; Tables S3 and S4). We examined the relative enrichment of synaptic proteins in the TNTP dataset compared with NHS-biotin-labeled proteins in the retina and the optic nerve (ON) and LGN transportomes (Schiapparelli et al., 2019). TNTPs are significantly enriched for synaptic proteins compared with the retina or the ON transportome, whereas TNTPs and the LGN transportome are enriched similarly for synaptic proteins (Figure 5A). SynGO (Koopmans et al., 2019) shows that TNTPS are annotated to pre- and postsynaptic compartments, with greater enrichment of presynaptic compartment categories (Figures 5C–5E). Given the distribution of biotin labeling in postsynaptic compartments (Figures 2, 3, S3, and S4), it is noteworthy that TNTPs are annotated to postsynaptic locations, including the cytosol and postsynaptic cytoskeleton. Gene Ontology functional categories and networks (Mi

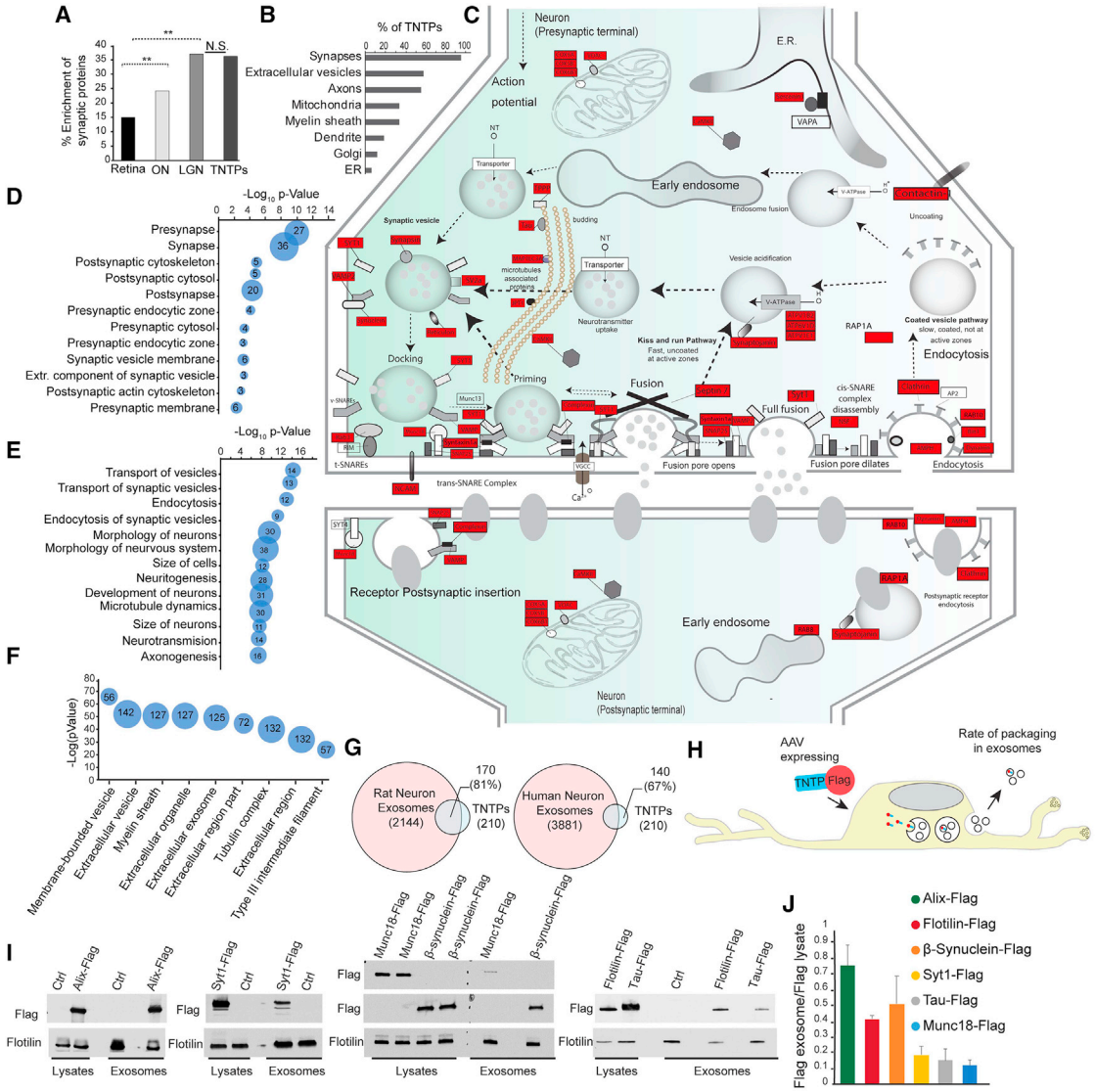

Figure 5. Proteomics analysis of TNTPs

(A) Synaptic protein enrichment in TNTPs compared with biotin-labeled proteins from the retina, ON, and LGN (Fisher's exact test, **p < 0.001; not significant [N.S.], p = 0.83366; retina versus TNTPs, Z = −5.8057; retina versus LGN, Z = −9.9772; TNTPs versus LGN, Z = 0.2085).

(B) Subcellular distribution of TNTPs.

(C) Schematic distribution of TNTPs (red) in pre- and postsynaptic compartments.

(D) Cellular compartment analysis using SynGO shows enrichment in synaptic proteins.

(E) Gene Ontology functional analysis indicates that TNTPs are involved in vesicle transport and endocytosis.

(F) TNTPs are annotated to exosomes.

(D and F) The y axis shows p values as −log. The number in the bubble is the number of TNTPs assigned to the bubble category, plotted on the x axis.

(G) The majority of TNTPs are present in exosome cargo from rat primary neuronal cultures (left) or from induced pluripotent stem cell (iPSC)-derived human neuronal cultures (right).

Data for (B) and (D)–(G) are shown in Table S3.

(H) Schematic of experiments to test whether TNTPs are released in neuronal exosomes.

(I) Western blots of FLAG and flotillin label in neuron lysates and exosomes, from left to right, from cultures expressing FLAG-tagged alix, synaptotagmin 1, Munc18, β-synuclein, flotillin, and tau.

(J) Relative packaging and release of exosome cargo. Neuronal exosomes contain FLAG-TNTPs, β-synuclein, synaptotagmin 1, tau, or Munc18. Alix, flotillin, and the TNTP β-synuclein, are packaged more efficiently into exosomes compared with tau, Munc18, and synaptotagmin 1. Data are plotted as mean ± SEM. n = 3.

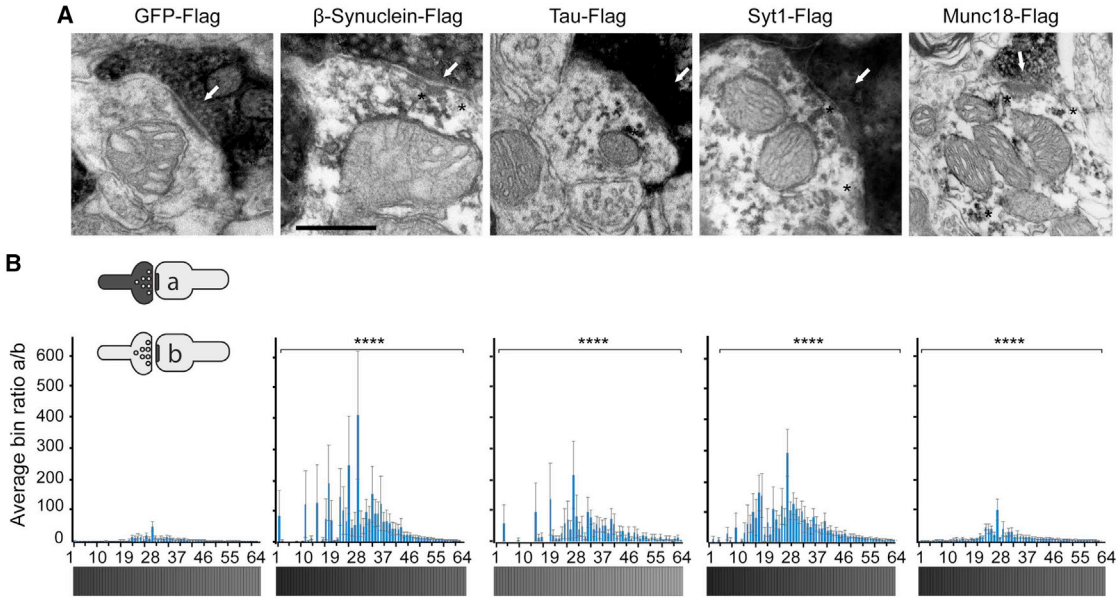

Figure 6. TNTPs transfer to LGN postsynaptic sites

(A) Images of EM sections showing retinogeniculate synapses (white arrows) with FLAG labeling in postsynaptic profiles in β-synuclein, tau, synaptotagmin 1 (Syt1), and Munc18 samples but not GFP. Scale bar, 500 nm.

(B) Pixel intensity histograms showing significant transfer of FLAG-labeled TNTPs from presynaptic to postsynaptic sites compared with the FLAG-GFP control. Pixel intensity histograms of labeled apposed postsynaptic profiles (a in the schematics) were normalized to unlabeled apposed postsynaptic profiles (b in the schematics) (see also STAR Methods). The LUT for the intensity scale is shown under the y axis. Data are plotted as mean ± SEM. n = 12 synapses for GFP-FLAG, 11 for synuclein-, 4 for tau-, 5 for Syt1-, and 8 for Munc18-FLAG. ****$p < 0.0001$, calculated by comparing ratio histograms of individual FLAG-TNTPs with FLAG-GFP using two-way ANOVA with Sidak correction for multiple comparisons.

et al., 2019) represented in the TNTPs indicate that TNTPs are involved in transport and endocytosis of synaptic vesicles (Figure 5E; Table S3). STRING (Search Tool for the Retrieval of Interacting Genes/Proteins) analysis indicates that TNTPs form interacting networks that mediate vesicle dynamics, cytoskeletal dynamics, regulation of post-translation modifications, and proteostasis (Figure S5F; Table S3). This analysis supports a model in which proteins are first transported to presynaptic retinogeniculate terminals, transferred to LGN relay neurons, and then transported to geniculocortical axons in the VC.

TNTP annotation to extracellular vesicles (Figures 5B and 5F; Table S3) suggests that TNTPs are exosome cargo. Indeed, the majority of TNTPs are detected in proteomes of exosomes released from human (Sharma et al., 2019) and rat neuronal cultures (Figure 5G). The TNTPs tau, α- and β-synuclein, syntaxin1A, synaptotagmin 1, CaMKII, Munc18, Bin-1, BASP-1, calbindin 2, and calmodulin are in neuronal exosomes (Figure S3G). To test whether TNTPs are released from neurons in exosomes, we infected primary neurons with AAV-expressing FLAG fusion proteins of the TNTPs β-synuclein, synaptotagmin 1, tau, or Munc18, and the exosome markers alix and flotillin (Figure 5H). All TNTP-FLAG constructs were detected in exosomes (Figure 5I). Furthermore, among the TNTPs, β-synuclein was packaged more efficiently than tau, Munc18, and synaptotagmin 1 (Figure 5J). These data indicate that exosome cargo includes TNTPs, that TNTPs are likely to be transported by exosomes, and that TNTPs are packaged differentially into exosomes.

TNTP transport in the visual system

To test whether TNTP transport between synaptically connected neurons can be detected directly *in vivo*, we virally expressed TNTP-FLAG constructs of synaptotagmin 1, Munc18, β-synuclein, and tau and a control construct, GFP-FLAG, in retinas. Immuno-EM demonstrated strong TNTP-FLAG immunolabeling in retinogeniculate presynaptic sites and in postsynaptic profiles of LGN dendrites in animals with retinal β-synuclein-, tau-, Munc18-, and synaptotagmin 1-FLAG expression (Figures 6A, S6C–S6G, S7A, and S7B). Quantifying transfer of FLAG-labeled TNTPs into postsynaptic sites, as described above, shows significant increases in label in postsynaptic profiles apposed to TNTP-FLAG presynaptic sites compared with GFP-FLAG (Figures 6B and S6H). Normalizing the individual TNTP data to GFP-FLAG indicates that the extent of TNTP transfer differs between TNTPs: β-synuclein > synaptotagmin 1 > tau > Munc18 (Figure S6I). The greater transfer of β-synuclein-FLAG may reflect the more robust packaging of β-synuclein in neuronal exosomes compared with other TNTPs (Figure 5J).

Using confocal microscopy, we observe TNTP-FLAG constructs but not GFP-FLAG in LGN neuronal cell bodies and geniculocortical axons (Figures 7A–7C and S7). We virally expressed β-synuclein-, synaptotagmin 1-, Munc18-, tau-, and GFP-FLAG in one eye and, after 12 days, prepared vibratome sections through the LGN ipsilateral and contralateral to the infected eye (Figure 7A). We detected FLAG-labeled puncta in LGN cell bodies for all TNTPs tested, but not GFP-FLAG (Figures 7B, 7C, S7C, and S7D; Videos S1, S2, and S3). To

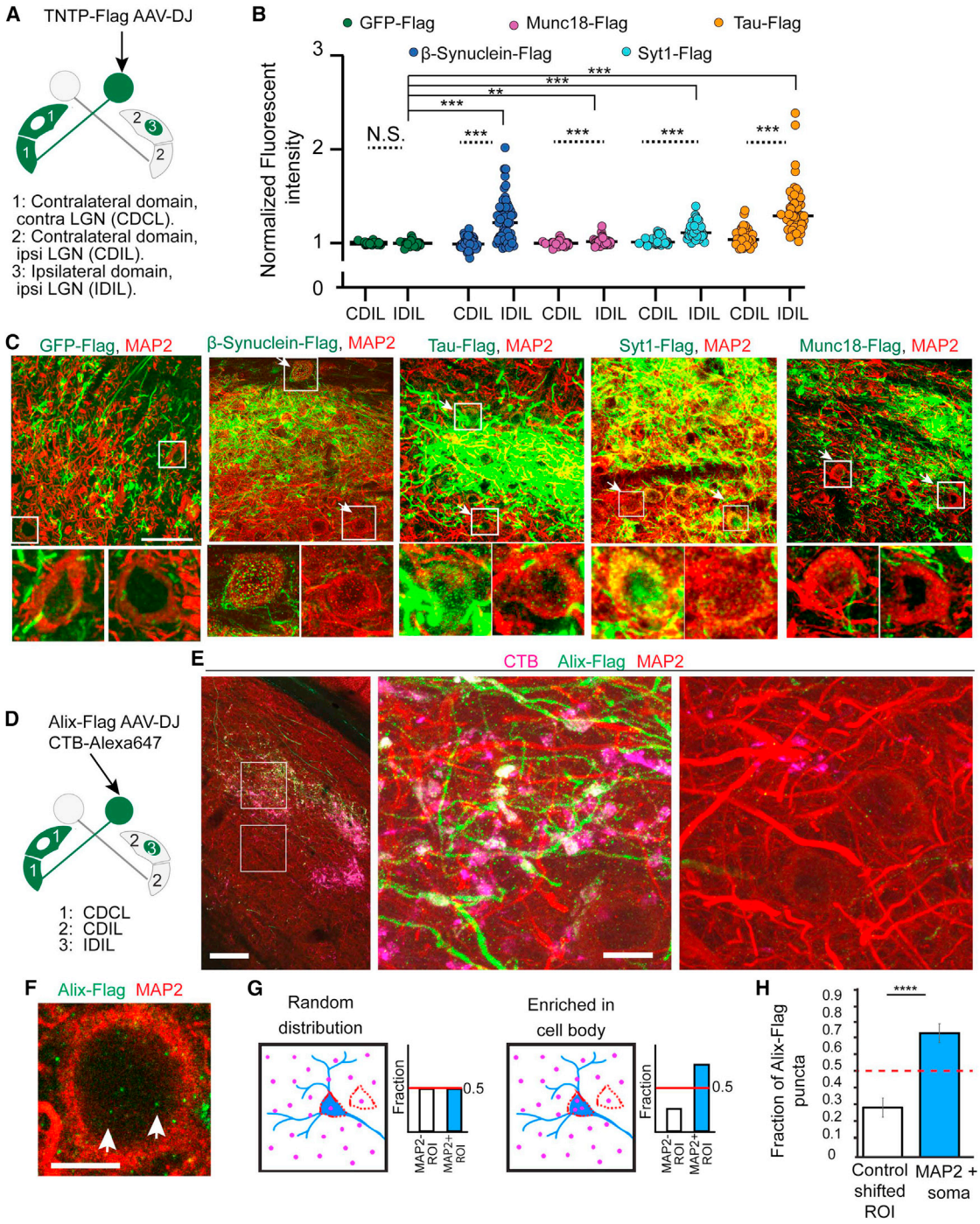

Figure 7. TNTPs are detected in LGN neurons

(A) Schematic of retinal projection domains in the ipsilateral and contralateral LGN following monocular labeling: (1) contralateral domain of the contralateral LGN (CDCL), (2) contralateral domain of the ipsilateral LGN (CDIL), and (3) ipsilateral domain in the ipsilateral LGN (IDIL).

(B and C) TNTP-FLAG, but not GFP-FLAG, is detected in LGN somata.

(B) Normalized FLAG intensity is significantly greater in LGN somata innervated by β-synuclein-, Munc18-, Syt1-, and tau-FLAG-expressing retinal inputs in the IDIL compared with the CDIL. The LGN innervated by GFP-FLAG inputs showed no significant differences between innervated and control regions of the LGN (Mann-Whitney *U* test.) Comparing TNTP-FLAG and GFP-FLAG in the IDIL shows significantly more transfer of TNTP-FLAG constructs. two-way ANOVA with Sidak correction for multiple comparisons; $^{**}p < 0.01$, $^{***}p < 0.001$, n = 3 animals; cell numbers (format: construct, IDIL, CDIL): GFP, 36, 33; β-syn, 59, 54; tau, 121, 84; syt1, 40, 34; munc18, 47, 45).

(C) Confocal images of an LGN expressing retinal FLAG-tagged TNTPs, as indicated, labeled with FLAG (green) and MAP2 (red) antibodies. The FLAG label identifies LGN regions that are densely innervated by the AAV-infected ipsilateral retina. White boxed areas, shown enlarged below, identify somata in which

(legend continued on next page)

quantify somatic TNTP-FLAG labeling, we first compared FLAG intensity in LGN somata, specifically in the ipsilateral projection domain of the ipsilateral LGN (IDIL), with the neighboring unlabeled region in the same images innervated by the contralateral eye, called the contralateral domain of the ipsilateral LGN (CDIL). This analysis detected β-synuclein-, tau-, Munc18-, and synaptotagmin 1-FLAG- but not GFP-FLAG-labeled puncta in LGN somata in the innervated domain compared with the control region (Figures 7A–7C). Furthermore, comparing TNTP constructs with GFP in the IDIL shows significantly more transfer of TNTP-FLAG constructs (Figure 7B). In a second analysis, we compared FLAG labeling in LGN somata in the contralateral domain of the contralateral LGN (CDCL), which receives direct retinal innervation, with the unlabeled CDIL. This analysis also detected TNTP-FLAG-labeled puncta, but not GFP-FLAG puncta, in the innervated LGN somata (Figures S7C and S7D). Furthermore, we detected β-synuclein-FLAG- and tau-FLAG-labeled axons in the VC 1 month after intravitreal AAV injection (Figure S7E). These data indicate that TNTPs transfer between neurons in the healthy intact brain, that transfer occurs at or near synapses, and that TNTPs can distribute to cell bodies and geniculocortical axons.

These results suggest that TNTPs may be developed as transsynaptic tools. We screened fusion proteins of cre recombinase and the TNTPs β-synuclein, Munc18, αCaMKII, syntaxin1A, and synaptotagmin 1 for transfer to neurons expressing floxed reporter protein and observed reporter expression in primary neuronal cultures, an *in vivo Xenopus* tadpole brain, and an *in vivo* rodent visual system (Figure S8). These data demonstrate that anterograde transfer of TNTP-cre recombinase drives reporter expression in recipient cells. In particular, β-synuclein-cre recombinase transfers from RGCs to LGN relay cells, where it is transported to the nucleus and induces reporter gene expression *in vivo* in the visual circuit in mammals.

Exosomes are involved in TNTP transport in the visual system

So far, our data show that the majority of TNTPs are neuronal exosome cargo, that TNTP-FLAG constructs are packaged into exosomes, and that they transfer between RGC axons and LGN neurons. Next we sought to visualize exosome transfer from RGC axons to LGN neurons. First we confirmed that retinal neurons release exosomes containing TNTP cargo, Munc18, syntaxin1, synaptotagmin 1, synucleins, and CaMKII as well as alix and flotillin (Figures S9A–S9I). We then expressed the exosome marker alix-FLAG in the retina to evaluate exosome release at retinogeniculate synapses using the strategy described above (Figures S2A–S2E, Figures 7A–7C). One eye was injected with CTB-Alexa 647 to label axons and AAV-expressing alix-FLAG, resulting in dense axonal labeling in a patch of the ipsilateral LGN (the IDIL) surrounded by unlabeled tissue that is innervated by the unlabeled contralateral eye (the CDIL) (Figure 7D). Immunolabeling LGN tissue sections for endogenous alix or alix-FLAG reveals alix-labeled puncta within RGC presynaptic boutons (Figures S9J–S9K) and alix-FLAG puncta outside of alix-FLAG-expressing RGC axons labeled with CTB (Figures 7E, 7F, and S9K), suggesting that alix-FLAG-containing exosomes may be released from RGC axons *in vivo*. Alix-FLAG-labeled puncta were readily detected in the LGN innervated by labeled axons but absent from surrounding areas without alix-FLAG-labeled axons, suggesting that FLAG+ puncta may originate from alix-FLAG+ axons (Figures 7E, 7G, and 7H). We compared areas in the LGN with dense alix-FLAG labeled RGC inputs (Figure 7E, center) with the neighboring areas innervated by the unlabeled axons from the contralateral eye (Figure 7E, right). Similar to observations with TNTP-FLAG, we observed alix-FLAG puncta within LGN neuronal cell bodies, identified by the characteristic MAP2+ immunolabeling (Figures 7E and 7F) in areas innervated by FLAG + axons, but not in unlabeled neighboring areas. Quantification of alix-FLAG puncta in regions of interest (ROIs) of MAP2+ cell bodies compared with control shifted ROIs indicates significant enrichment of alix-FLAG puncta in MAP2+ cell bodies (Figures 7G and 7H). These results indicate that alix-FLAG is packaged into exosomes with endogenous exosome cargo and co-localizes with endogenous alix in puncta in retinogeniculate boutons. Furthermore, LGN neurons incorporate the exosome reporter (alix-FLAG) expressed in RGC axons. Importantly, the presence of alix-FLAG in LGN neuronal cell bodies, similar to our data showing TNTP in LGN neuronal cell bodies (Figures 7A–7C, S7C, and S7D), provides strong evidence that TNTPs transfer between neurons via exosomes.

FLAG labeled puncta for β-synuclein, Syt1, and tau constructs correlate with the extent of innervation with the TNTP-FLAG construct. Images are saturated for FLAG labeling to enable visualization of TNTP-FLAG-labeled puncta in somata. Scale bar, 50 μm. See also Videos S1, S2, and S3.

(D–H) LGN somata label with alix-FLAG expressed in RGCs.

(D) Schematic of the experiment: monocular labeling with alix-FLAG and CTB-Alexa 647 to label RGC projections.

(E) Alix-FLAG in retinogeniculate axons and puncta outside of axons. Left: low-magnification image of the LGN ipsilateral to the labeled eye. Alix-FLAG (green) and CTB (magenta) show co-labeling of axonal projections and boutons in the IDIL (top white box), neighboring the unlabeled CDIL (bottom white box; regions 2 and 3 in D), shown at higher magnification in the center and right panels, respectively. Scale bar, 100 μm. Center: alix-FLAG puncta (green) outside of labeled RGC boutons colocalize with MAP2+ (red) somata and processes close to RGC axonal projections. Scale bar, 5 μm. Right: image of the adjacent CDIL, showing few or no alix-FLAG puncta.

(F) MAP2+ somata in areas innervated by alix-FLAG-labeled RGC axons contain alix-FLAG puncta (white arrows). Scale bar, 5 μm.

(G) Schematic of the analysis to quantify punctum enrichment in MAP2+ somata. If punctum distribution were random (left), then the fraction of puncta in regions of interest (ROIs) around MAP2+ cell bodies (MAP2+ ROIs) and the ROIs shifted out of the MAP2+ cell body (MAP2− ROIs) would be 0.5 for each ROI. If puncta were enriched in ROIs of MAP2-labeled somata compared with the surrounding area, then the fraction of puncta in MAP2+ ROIs would be significantly higher than the fraction of puncta in MAP2− ROIs (right).

(H) Enrichment of alix-FLAG puncta in ROIs of MAP2+ somata compared with control shifted ROIs. n = 5 animals, 21 cells. $p \leq 0.0001$, two-tailed Mann-Whitney Wilcoxon test.

DISCUSSION

Protein transport between neurons has been reported in a few cases but is thought to be a relatively rare event. Using *in vivo* biotinylation of endogenous proteins together with a strategy to enrich and directly identify biotinylated peptides using DiDBiT and MS/MS (Schiapparelli et al., 2014), we demonstrated that transfer of TNTPs between synaptically connected neurons in the visual circuit occurs on a larger scale than previously appreciated, with ~200 endogenous TNTPs recovered from geniculocortical axons in the VC and identified with MS/MS proteomics. A bioinformatics analysis indicates that 95% of TNTPs are annotated to synapses and that 80% of TNTPs are exosome cargo. Using light microscopy and EM, we show that TNTPs are selectively transferred from RGC presynaptic sites to excitatory but not inhibitory postsynaptic LGN neurons. TNTP-FLAG constructs expressed in the retina are transported across retinogeniculate synapses, followed by intraneuronal distribution through LGN neuronal dendrites, somata, and geniculocortical axons. Finally, using expression of the β-synuclein-cre recombinase fusion protein, we demonstrate the ability of TNTPs to transport cre recombinase across synapses and to induce gene expression in postsynaptic neurons. These data demonstrate the non-pathological transport of diverse endogenous proteins across specific synapses in the brain, identity the proteins transported across retinogeniculate synapses and their potential mechanism of transport by exosomes, and establish the feasibility of hijacking this communication to manipulate postsynaptic gene expression in a circuit-specific manner.

TNTPs are detected in LGN neurons by light microscopy and EM

Labeling retinal proteins with NHS-biotin consistently resulted in biotinylated protein in LGN dendrites adjacent to densely labeled RGC boutons, with punctate biotinylated protein labeling associating with microtubules, dendritic spines, and shafts and around cell nuclei in postsynaptic neurons. As validation, we demonstrated comparable distribution of TNTPs tagged with FLAG. The association of TNTP labeling with postsynaptic endosome-like vesicles and tubular-vesicular structures that are usually associated with sorting endosomes (Kennedy and Ehlers, 2006) suggests a potential role of endocytic machinery in internalization of TNTPs, as described for exogenously labeled proteins (Cooney et al., 2002).

Previous studies of protein transport in the visual system labeled proteins by incorporation of radiolabeled amino acids during *de novo* protein synthesis *in vivo* (Grafstein, 1971; Grafstein and Laureno, 1973). This approach could not determine whether few or many proteins could be engaged in this sort of transport or distinguish between transneuronal transfer of radiolabeled proteins or free amino acids released by RGC axons and incorporated into new proteins in LGN neurons (Kanold and Shatz, 2006). To answer these questions, we used a chemical labeling strategy in which the tag cannot re-incorporate into other proteins after protein degradation. Furthermore, we developed an unbiased method to quantify labeled protein in immuno-EM samples and used this analysis to demonstrate that endogenous proteins are transported to postsynaptic neurons in the LGN and then into geniculocortical axons in the VC in the adult rat.

TNTPs transfer selectively to excitatory but not inhibitory LGN neurons

We analyzed transfer of biotinylated proteins in serial EM sections through LGN glomeruli, which contain triads of RGC boutons, postsynaptic geniculocortical relay cells, and inhibitory GABAergic neurons (Sherman, 2004). The majority of biotin-labeled postsynaptic dendrites were excitatory, suggesting specificity of transneuronal transport to geniculocortical relay cells. The observation that single presynaptic sites direct protein transport to excitatory postsynaptic sites but not neighboring inhibitory sites suggests that cell-type-specific transport is achieved by specificity in uptake mechanisms. Future work dissecting the molecular organization of surface proteins at different synaptic clefts will provide more insight into this (Loh et al., 2016).

TNTPs are exosome cargo and include synaptic and axonal proteins

TNTPs recovered from the VC are enriched in axonally localized proteins, likely because our anatomy-based purification strategy required TNTPs to be transported into geniculocortal axons. We did not analyze TNTPs that remained within the somatodendritic compartment of geniculocortical neurons, suggesting that still unidentified somatodendritic TNTPs may include different categories of proteins than those transported into axons. Proteins involved in regulation of vesicular transport and endocytosis, neuronal development, axonogenesis, and neuronal architecture were highly represented among TNTPs, including several growth factors and growth-related proteins. These ontologies suggest that TNTPs may provide anterograde signals that maintain circuit connectivity and function. Consistent with this hypothesis, ON transection or glaucoma lead to progressive apoptosis of neurons in the LGN and VC (You et al., 2012) with concomitant plastic changes in neuronal activation in the VC (Vasalauskaite et al., 2019). This progressive loss of relay cells is preceded by AKT dephosphorylation in the LGN and VC (You et al., 2012). One hypothesis is that TNTPs affect the function of the AKT pathway and that decreased transneuronal transport leads to hypofunction of this signaling pathway. Supporting this hypothesis, one of the TNTPs is PIN1, which is involved in AKT activation (Liao et al., 2009; Zhang et al., 2019).

The majority of TNTPs are neuronal exosome cargo. Exosomes mediate intercellular communication between neurons and other cell types in the nervous system, and intercellular signaling mediated by transfer of exosome cargo regulates synapse formation, circuit assembly, and a range of physiological functions (Budnik et al., 2016; Rajendran et al., 2014; Sharma et al., 2013, 2019). For instance, anterograde exosome-mediated transfer of Wnt and Syt4 is required for development of the *Drosophila* neuromuscular junction (Korkut et al., 2009, 2013). Our previous quantitative proteomics comparison of exosomes released from hiPSC-derived neural cultures lacking MECP2 and isogenic control cultures demonstrated that control exosomes contain multiple functional signaling networks known

to be important for neuronal circuit development and that treating MECP2 knockdown human primary neural cultures with control exosomes rescued deficits in neuronal development, synaptogenesis, and circuit activity (Sharma et al., 2019). Considering that TNTPs include many synaptic proteins, including SNARE proteins, syntaxin, synaptobrevin 2, synaptotagmin 1, and SNAP 25, it is interesting that that exosome-mediated delivery of synaptobrevin 2 led to its incorporation into synaptic vesicles and partial restoration of synaptic transmission in synaptobrevin 2 knockout neurons (Vilcaes et al., 2021), suggesting that TNTP transfer affects synaptic function in recipient neurons. Complementing recent studies showing that release of GFP-tagged exosomes from cells in the brain results in GFP-labeled puncta in the tissue (McCann et al., 2020), we find that retinal expression of FLAG-tagged alix, which is packaged into exosomes with endogenous TNTP cargo, resulted in alix-FLAG-labeled puncta in LGN dendrites, somata, and intracellular vesicular structures, similar to the distribution of the NHS-biotin label and TNTP-FLAG. These data provide support for the hypothesis of transfer of TNTPs between synaptically connected neurons, suggest that *in vivo* intercellular transport of TNTPs is mediated by exosomes, and demonstrate that exosome-mediated interneuronal transport can affect neuron development and function across species.

Anterograde transport of TNTP-cre recombinase drives gene expression in neuronal circuits

The observation that exogenously administered TNTP-FLAG is capable of transneuronal transport provides an opportunity to deliver proteins of interest fused to TNTPs to targeted postsynaptic neurons in a circuit in the intact animal. We demonstrate further flexibility of this system using expression of the β-synuclein cre recombinase fusion protein to drive gene expression in postsynaptic neurons *in vitro* and *in vivo* in *Xenopus* and mice, indicating that these are useful experimental systems in which to optimize anterograde tracer reagents. The sparse *in vivo* reporter labeling suggests that β-synuclein-cre recombinase transfer between neurons is low, likely because the nuclear localization signal in the cre recombinase pulls the β-synuclein-cre recombinase fusion protein into the donor cell nucleus and decreases transneuronal transport. Indeed, different features or protein motifs in TNTPs likely affect efficiency of transneuronal transport and nuclear targeting for cre-recombination and reporter expression in recipient neurons. Synucleins are highly enriched in presynaptic terminals (Jakes et al., 1994; Quilty et al., 2003; Schiapparelli et al., 2019) but also in the cytosol and nucleus (Maroteaux et al., 1988; Mori et al., 2002; Specht et al., 2005; Yu et al., 2007). The bifunctional properties of the β-synuclein-cre recombinase fusion protein can be attributed to the synaptic targeting and transsynaptic transport properties of β-synuclein and the nuclear import and gene regulation properties of cre recombinase. Although our initial experiments provide a proof of principle showing that TNTPs could be used to generate anterograde transsynaptic labeling tools applicable to study circuits in diverse species, additional protein engineering is required to optimize interneuronal transport and the capacity to drive reporter expression of TNTP-based transsynaptic anterograde circuit labeling tools. β-Synuclein-cre recombinase remains a promising candidate; for instance, if the cre recombinase nuclear localization signal could be transiently shielded in the donor cell until the fusion protein is safely packaged into exosomes. When in the postsynaptic recipient cell, the exposed nuclear localization signal in the cre recombinase would target the fusion protein to the nucleus.

TNTP variants are involved in mediating pathological processes

We identified α- and β-synuclein and tau among the TNTPs, indicating that these endogenous proteins were biotinylated in RGC somata and transported to retinogeniculate synapses, where they were selectively transferred to excitatory LGN relay neurons in the healthy visual circuit. Toxic forms of these proteins have been studied extensively in the context of neurodegenerative diseases and have been shown to propagate through the brain, following stereotypical patterns that correlate with neuronal connectivity (Bieri et al., 2017; Braak et al., 2003; Brettschneider et al., 2015; de Calignon et al., 2012; Liu et al., 2012). Recent reports indicate that exosomes transport hyperphosphorylated tau and α-synuclein between neurons (Emmanouilidou et al., 2010; Wang et al., 2017) and that interneuronal exosome-mediated hyperphosphorylated tau transfer increases with neuronal activity (Pooler et al., 2013), consistent with evidence showing that exosome release increases with neuronal activity (Lachenal et al., 2011). Our observation of exosome-mediated transport of hundreds of functionally diverse proteins between specific synaptically connected neurons in the visual circuit suggests that anterograde transneuronal protein transport is an underappreciated component of cell-to-cell communication that may contribute to a range of physiological processes in healthy brain circuits.

Limitations of the study

The main challenge of this study was to identify candidate proteins that cross synapses from RGCs to LGN neurons. After demonstrating that NHS-biotin-labeled retinal proteins are detected in the LGN and cortex using biochemical and histological methods, we used unbiased MS/MS to identify TNTPs from the VC. MS/MS does not include amplification, like RNA sequencing (RNA-seq), likely undersampling TNTPs. Because we only analyzed TNTPs from geniculocortical axons, TNTPs that were retained in LGN dendrites and cell bodies were not sampled. Quantifying TNTP enrichment in the VC by western blots is challenging when the differences in labeled protein are large, as in our samples. A remaining challenge is to identify function(s) of intercellularly transported proteins.

STAR★METHODS

Detailed methods are provided in the online version of this paper and include the following:

- KEY RESOURCES TABLE
- RESOURCE AVAILABILITY
  - Lead contact
  - Materials availability
  - Data and code availability

SUPPLEMENTAL INFORMATION

Supplemental information can be found online at https://doi.org/10.1016/j.celrep.2021.110287.

ACKNOWLEDGMENTS

This work was supported by NIH DP10D000458, R01EY011261, R01EY027437, P30EY019005, R01MH103134, and R01EY031597 and the Hahn Family Foundation (to H.T.C.); The Harold L. Dorris Neurosciences Center Endowment Fund (to H.-Y.H. and P.S.); P41GM103533 and R01MH067880 (to J.R.Y.); P30-EY026877 and Research to Prevent Blindness, Inc. to J.L.G; and U01EY027261 (to J.L.G., J.R.Y., and H.T.C.). We thank the Cline lab for helpful discussions and Robin Sung-kyu Park for help with bioinformatics analysis.

AUTHOR CONTRIBUTIONS

L.M.S. and H.T.C. conceived the study. L.M.S., P.S., J.L., H.-Y.H., and H.T.C. designed the experiments. L.M.S., J.L., H.-Y.H., P.S., H.-H.L., D.B.M., and Y.M. conducted experiments and data analysis. H.T.C., J.L.G., and J.R.Y. provided project mentorship. L.M.S., H.T.C., P.S., and S.H.S. wrote the manuscript with contributions from all authors.

DECLARATION OF INTERESTS

P.S. is the founder of and has equity interest in Xosomix, a biotechnology company dedicated to developing exosome-based diagnostics and therapeutics. The terms of this arrangement are in compliance with conflict-of-interest policies of Scripps Research.

Received: February 23, 2021
Revised: November 22, 2021
Accepted: December 28, 2021
Published: January 25, 2022

REFERENCES

Altar, C.A., Cai, N., Bliven, T., Juhasz, M., Conner, J.M., Acheson, A.L., Lindsay, R.M., and Wiegand, S.J. (1997). Anterograde transport of brain-derived neurotrophic factor and its role in the brain. Nature *389*, 856–860. https://doi.org/10.1038/39885.

Ashburner, M., Ball, C.A., Blake, J.A., Botstein, D., Butler, H., Cherry, J.M., Davis, A.P., Dolinski, K., Dwight, S.S., Eppig, J.T., et al. (2000). Gene ontology: tool for the unification of biology. The Gene Ontology Consortium. Nat. Genet. *25*, 25–29. https://doi.org/10.1038/75556.

Beaulieu, C., and Cynader, M. (1992). Preferential innervation of immunoreactive choline acetyltransferase synapses on relay cells of the cat's lateral geniculate nucleus: a double-labelling study. Neuroscience *47*, 33–44.

Bestman, J.E., Lee-Osbourne, J., and Cline, H.T. (2012). In vivo time-lapse imaging of cell proliferation and differentiation in the optic tectum of Xenopus laevis tadpoles. J. Comp. Neurol. *520*, 401–433. https://doi.org/10.1002/cne.22795.

Bickford, M.E., Slusarczyk, A., Dilger, E.K., Krahe, T.E., Kucuk, C., and Guido, W. (2010). Synaptic development of the mouse dorsal lateral geniculate nucleus. J. Comp. Neurol. *518*, 622–635. https://doi.org/10.1002/cne.22223.

Bieri, G., Gitler, A.D., and Brahic, M. (2017). Internalization, axonal transport and release of fibrillar forms of alpha-synuclein. Neurobiol. Dis. https://doi.org/10.1016/j.nbd.2017.03.007.

Binder, J.X., Pletscher-Frankild, S., Tsafou, K., Stolte, C., O'Donoghue, S.I., Schneider, R., and Jensen, L.J. (2014). COMPARTMENTS: unification and visualization of protein subcellular localization evidence. Database (Oxford) *2014*. https://doi.org/10.1093/database/bau012.

Braak, H., Del Tredici, K., Rub, U., de Vos, R.A., Jansen Steur, E.N., and Braak, E. (2003). Staging of brain pathology related to sporadic Parkinson's disease. Neurobiol. Aging *24*, 197–211.

Brettschneider, J., Del Tredici, K., Lee, V.M., and Trojanowski, J.Q. (2015). Spreading of pathology in neurodegenerative diseases: a focus on human studies. Nat. Rev. Neurosci. *16*, 109–120. https://doi.org/10.1038/nrn3887.

Budnik, V., Ruiz-Canada, C., and Wendler, F. (2016). Extracellular vesicles round off communication in the nervous system. Nat. Rev. Neurosci. *17*, 160–172. https://doi.org/10.1038/nrn.2015.29.

Cardin, J.A., Carlen, M., Meletis, K., Knoblich, U., Zhang, F., Deisseroth, K., Tsai, L.H., and Moore, C.I. (2010). Targeted optogenetic stimulation and recording of neurons in vivo using cell-type-specific expression of Channelrhodopsin-2. Nature protocols *5*, 247–254. https://doi.org/10.1038/nprot.2009.228.

Cooney, J.R., Hurlburt, J.L., Selig, D.K., Harris, K.M., and Fiala, J.C. (2002). Endosomal compartments serve multiple hippocampal dendritic spines from a widespread rather than a local store of recycling membrane. J. Neurosci. *22*, 2215–2224.

de Calignon, A., Polydoro, M., Suarez-Calvet, M., William, C., Adamowicz, D.H., Kopeikina, K.J., Pitstick, R., Sahara, N., Ashe, K.H., Carlson, G.A., et al. (2012). Propagation of tau pathology in a model of early Alzheimer's disease. Neuron *73*, 685–697, S0896-6273(12)00038-4 [pii]. https://doi.org/10.1016/j.neuron.2011.11.033.

Elfarrash, S., Jensen, N.M., Ferreira, N., Betzer, C., Thevathasan, J.V., Diekmann, R., Adel, M., Omar, N.M., Boraie, M.Z., Gad, S., et al. (2019). Organotypic slice culture model demonstrates inter-neuronal spreading of alpha-synuclein aggregates. Acta Neuropathol. Commun. *7*, 213. https://doi.org/10.1186/s40478-019-0865-5.

Emmanouilidou, E., Melachroinou, K., Roumeliotis, T., Garbis, S.D., Ntzouni, M., Margaritis, L.H., Stefanis, L., and Vekrellis, K. (2010). Cell-produced alpha-synuclein is secreted in a calcium-dependent manner by exosomes and impacts neuronal survival. J. Neurosci. *30*, 6838–6851. https://doi.org/10.1523/jneurosci.5699-09.2010.

Erisir, A., Van Horn, S.C., and Sherman, S.M. (1998). Distribution of synapses in the lateral geniculate nucleus of the cat: differences between laminae A and A1 and between relay cells and interneurons. J. Comp. Neurol. *390*, 247–255.

Grafstein, B. (1971). Transneuronal transfer of radioactivity in the central nervous system. Science *172*, 177–179.

Grafstein, B., and Forman, D.S. (1980). Intracellular transport in neurons. Physiol. Rev. *60*, 1167–1283. https://doi.org/10.1152/physrev.1980.60.4.1167.

Grafstein, B., and Laureno, R. (1973). Transport of radioactivity from eye to visual cortex in the mouse. Exp. Neurol. *39*, 44–57.

Grimm, D., Lee, J.S., Wang, L., Desai, T., Akache, B., Storm, T.A., and Kay, M.A. (2008). In vitro and in vivo gene therapy vector evolution via multispecies interbreeding and retargeting of adeno-associated viruses. J. Virol. *82*, 5887–5911. https://doi.org/10.1128/JVI.00254-08.

Haas, K., Jensen, K., Sin, W.C., Foa, L., and Cline, H.T. (2002). Targeted electroporation in Xenopus tadpoles in vivo–from single cells to the entire brain. Differ. Res. Biol. Divers. *70*, 148–154. https://doi.org/10.1046/j.1432-0436.2002.700404.x.

Hansen, C., and Li, J.Y. (2012). Beyond alpha-synuclein transfer: pathology propagation in Parkinson's disease. Trends Mol. Med. *18*, 248–255. https://doi.org/10.1016/j.molmed.2012.03.002.

Harris, K.M., and Weinberg, R.J. (2012). Ultrastructure of synapses in the mammalian brain. Cold Spring Harb Perspect. Biol. *4*. https://doi.org/10.1101/cshperspect.a005587.

Jakes, R., Spillantini, M.G., and Goedert, M. (1994). Identification of two distinct synucleins from human brain. FEBS Lett. *345*, 27–32.

Kanehisa, M. (2000). Pathway databases and higher order function. Adv. Protein Chem. *54*, 381–408.

Kanold, P.O., and Shatz, C.J. (2006). Subplate neurons regulate maturation of cortical inhibition and outcome of ocular dominance plasticity. Neuron *51*, 627–638. https://doi.org/10.1016/j.neuron.2006.07.008.

Kara, E., Marks, J.D., and Aguzzi, A. (2018). Toxic protein spread in neurodegeneration: reality versus fantasy. Trends Mol. Med. *24*, 1007–1020. https://doi.org/10.1016/j.molmed.2018.09.004.

Kennedy, M.J., and Ehlers, M.D. (2006). Organelles and trafficking machinery for postsynaptic plasticity. Annu. Rev. Neurosci. *29*, 325–362. https://doi.org/10.1146/annurev.neuro.29.051605.112808.

Koopmans, F., van Nierop, P., Andres-Alonso, M., Byrnes, A., Cijsouw, T., Coba, M.P., Cornelisse, L.N., Farrell, R.J., Goldschmidt, H.L., Howrigan, D.P., et al. (2019). SynGO: an evidence-based, expert-curated knowledge base for the synapse. Neuron *103*, 217–234 e4. https://doi.org/10.1016/j.neuron.2019.05.002.

Korkut, C., Ataman, B., Ramachandran, P., Ashley, J., Barria, R., Gherbesi, N., and Budnik, V. (2009). Trans-synaptic transmission of vesicular Wnt signals through Evi/Wntless. Cell *139*, 393–404, S0092-8674(09)01047-2 [pii]. https://doi.org/10.1016/j.cell.2009.07.051.

Korkut, C., Li, Y., Koles, K., Brewer, C., Ashley, J., Yoshihara, M., and Budnik, V. (2013). Regulation of postsynaptic retrograde signaling by presynaptic exosome release. Neuron *77*, 1039–1046. https://doi.org/10.1016/j.neuron.2013.01.013.

Lachenal, G., Pernet-Gallay, K., Chivet, M., Hemming, F.J., Belly, A., Bodon, G., Blot, B., Haase, G., Goldberg, Y., and Sadoul, R. (2011). Release of exosomes from differentiated neurons and its regulation by synaptic glutamatergic activity. Mol. Cell. Neurosci. *46*, 409–418. https://doi.org/10.1016/j.mcn.2010.11.004.

Lavallee-Adam, M., Park, S.K., Martinez-Bartolome, S., He, L., and Yates, J.R., 3rd. (2015). From raw data to biological discoveries: a computational analysis pipeline for mass spectrometry-based proteomics. J Am Soc Mass Spectrom *26*, 1820–1826.

Li, J., Wang, S., and Bickford, M.E. (2003). Comparison of the ultrastructure of cortical and retinal terminals in the rat dorsal lateral geniculate and lateral posterior nuclei. J. Comp. Neurol. *460*, 394–409. https://doi.org/10.1002/cne.10646.

Liao, L.J., McClatchy, D.B., and Yates, J.R. (2009). Shotgun proteomics in neuroscience. Neuron *63*, 12–26. https://doi.org/10.1016/j.neuron.2009.06.011.

Liu, H.H., McClatchy, D.B., Schiapparelli, L., Shen, W., Yates, J.R., 3rd, and Cline, H.T. (2018). Role of the visual experience-dependent nascent proteome in neuronal plasticity. eLife *7*. https://doi.org/10.7554/eLife.33420.

Liu, L., Drouet, V., Wu, J.W., Witter, M.P., Small, S.A., Clelland, C., and Duff, K. (2012). Trans-synaptic spread of tau pathology in vivo. PLoS one *7*, e31302. https://doi.org/10.1371/journal.pone.0031302 PONE-D-11-23353.

Loh, K.H., Stawski, P.S., Draycott, A.S., Udeshi, N.D., Lehrman, E.K., Wilton, D.K., Svinkina, T., Deerinck, T.J., Ellisman, M.H., Stevens, B., et al. (2016). Proteomic analysis of unbounded cellular compartments: synaptic clefts. Cell *166*, 1295–1307 e1. https://doi.org/10.1016/j.cell.2016.07.041.

Madisen, L., Zwingman, T.A., Sunkin, S.M., Oh, S.W., Zariwala, H.A., Gu, H., Ng, L.L., Palmiter, R.D., Hawrylycz, M.J., Jones, A.R., et al. (2010). A robust and high-throughput Cre reporting and characterization system for the whole mouse brain. Nat. Neurosci. *13*, 133–140. https://doi.org/10.1038/nn.2467.

Maroteaux, L., Campanelli, J.T., and Scheller, R.H. (1988). Synuclein: a neuron-specific protein localized to the nucleus and presynaptic nerve terminal. J. Neurosci. *8*, 2804–2815.

McCann, J.V., Bischoff, S.R., Zhang, Y., Cowley, D.O., Sanchez-Gonzalez, V., Daaboul, G.D., and Dudley, A.C. (2020). Reporter mice for isolating and auditing cell type-specific extracellular vesicles in vivo. Genesis *58*, e23369. https://doi.org/10.1002/dvg.23369.

McKay, B.E., Molineux, M.L., and Turner, R.W. (2008). Endogenous biotin in rat brain: implications for false-positive results with avidin-biotin and streptavidin-biotin techniques. Methods Mol. Biol. (Clifton, N.J.) *418*, 111–128.

Mi, H., Muruganujan, A., Ebert, D., Huang, X., and Thomas, P.D. (2019). PANTHER version 14: more genomes, a new PANTHER GO-slim and improvements in enrichment analysis tools. Nucleic Acids Res. *47*, D419–D426. https://doi.org/10.1093/nar/gky1038.

Montero, V.M., and Singer, W. (1985). Ultrastructural identification of somata and neural processes immunoreactive to antibodies against glutamic acid decarboxylase (GAD) in the dorsal lateral geniculate nucleus of the cat. Exp. Brain Res. *59*, 151–165.

Mori, F., Tanji, K., Yoshimoto, M., Takahashi, H., and Wakabayashi, K. (2002). Immunohistochemical comparison of alpha- and beta-synuclein in adult rat central nervous system. Brain Res. *941*, 118–126.

Paxinos, G., and Watson, C. (1998). The Rat Brain in Stereotaxic Coordinates (Academic Press).

Pielot, R., Smalla, K.H., Muller, A., Landgraf, P., Lehmann, A.C., Eisenschmidt, E., Haus, U.U., Weismantel, R., Gundelfinger, E.D., and Dieterich, D.C. (2012). SynProt: a database for proteins of detergent-resistant synaptic protein preparations. Front. Synap. Neurosci. *4*, 1. https://doi.org/10.3389/fnsyn.2012.00001.

Pirooznia, M., Wang, T., Avramopoulos, D., Valle, D., Thomas, G., Huganir, R.L., Goes, F.S., Potash, J.B., and Zandi, P.P. (2012). SynaptomeDB: an ontology-based knowledgebase for synaptic genes. Bioinformatics *28*, 897–899. https://doi.org/10.1093/bioinformatics/bts040.

Pooler, A.M., Phillips, E.C., Lau, D.H., Noble, W., and Hanger, D.P. (2013). Physiological release of endogenous tau is stimulated by neuronal activity. EMBO Rep. *14*, 389–394. https://doi.org/10.1038/embor.2013.15.

Quilty, M.C., Gai, W.P., Pountney, D.L., West, A.K., and Vickers, J.C. (2003). Localization of alpha-, beta-, and gamma-synuclein during neuronal development and alterations associated with the neuronal response to axonal trauma. Exp. Neurol. *182*, 195–207.

Rajendran, L., Bali, J., Barr, M.M., Court, F.A., Kramer-Albers, E.M., Picou, F., Raposo, G., van der Vos, K.E., van Niel, G., Wang, J., and Breakefield, X.O. (2014). Emerging roles of extracellular vesicles in the nervous system. J. Neurosci. *34*, 15482–15489. https://doi.org/10.1523/JNEUROSCI.3258-14.2014.

Reinis, S., and Goldman, J.M. (1984). The transneuronal transport of proline within the mouse visual system: some characteristics of the [3H]-proline containing material. Brain Res. Bull. *12*, 339–342.

Rhodes, C.H., and Gonatas, N.K. (1986). Lectin affinity and PAGE analysis of soluble axonally transported glycoconjugates in the rat visual system. Brain Res. *399*, 42–50.

Schiapparelli, L.M., McClatchy, D.B., Liu, H.H., Sharma, P., Yates, J.R., 3rd, and Cline, H.T. (2014). Direct detection of biotinylated proteins by mass

spectrometry. J. Proteome Res. *13*, 3966–3978. https://doi.org/10.1021/pr5002862.

Schiapparelli, L.M., Shah, S.H., Ma, Y., McClatchy, D.B., Sharma, P., Li, J., Yates, J.R., 3rd, Goldberg, J.L., and Cline, H.T. (2019). The retinal ganglion cell transportome identifies proteins transported to axons and presynaptic compartments in the visual system in vivo. Cell Rep. *28*, 1935–1947 e5. https://doi.org/10.1016/j.celrep.2019.07.037.

Schikorski, T. (2010). Pre-embedding immunogold localization of antigens in mammalian brain slices. Methods Mol. Biol. (Clifton, N.J.) *657*, 133–144. https://doi.org/10.1007/978-1-60761-783-9_10.

Sharma, P., Mesci, P., Carromeu, C., McClatchy, D.R., Schiapparelli, L., Yates, J.R., 3rd, Muotri, A.R., and Cline, H.T. (2019). Exosomes regulate neurogenesis and circuit assembly. Proc. Natl. Acad. Sci. U S A. *116*, 16086–16094. https://doi.org/10.1073/pnas.1902513116.

Sharma, P., Schiapparelli, L., and Cline, H.T. (2013). Exosomes function in cell-cell communication during brain circuit development. Curr. Opin. Neurobiol. *23*, 997–1004. https://doi.org/10.1016/j.conb.2013.08.005.

Sherman, S.M. (2004). Interneurons and triadic circuitry of the thalamus. Trends Neurosc. *27*, 670–675. https://doi.org/10.1016/j.tins.2004.08.003.

Spatazza, J., Lee, H.H., Di Nardo, A.A., Tibaldi, L., Joliot, A., Hensch, T.K., and Prochiantz, A. (2013). Choroid-plexus-derived Otx2 homeoprotein constrains adult cortical plasticity. Cell Rep. *3*, 1815–1823. https://doi.org/10.1016/j.celrep.2013.05.014.

Specht, C.G., Tigaret, C.M., Rast, G.F., Thalhammer, A., Rudhard, Y., and Schoepfer, R. (2005). Subcellular localisation of recombinant alpha- and gamma-synuclein. Mol. Cell. Neurosci. *28*, 326–334. https://doi.org/10.1016/j.mcn.2004.09.017.

Specht, S., and Grafstein, B. (1973). Accumulation of radioactive protein in mouse cerebral cortex after injection of 3H-fucose into the eye. Exp. Neurol. *41*, 705–722.

Sugiyama, S., Di Nardo, A.A., Aizawa, S., Matsuo, I., Volovitch, M., Prochiantz, A., and Hensch, T.K. (2008). Experience-dependent transfer of Otx2 homeoprotein into the visual cortex activates postnatal plasticity. Cell *134*, 508–520, S0092-8674(08)00839-8 [pii]. https://doi.org/10.1016/j.cell.2008.05.054.

Szklarczyk, D., Morris, J.H., Cook, H., Kuhn, M., Wyder, S., Simonovic, M., Santos, A., Doncheva, N.T., Roth, A., Bork, P., et al. (2017). The STRING database in 2017: quality-controlled protein-protein association networks, made broadly accessible. Nucleic Acids Res. *45*, D362–D368. https://doi.org/10.1093/nar/gkw937.

The Gene Ontology, C. (2019). The gene ontology resource: 20 years and still GOing strong. Nucleic Acids Res. *47*, D330–D338. https://doi.org/10.1093/nar/gky1055.

Thomas, P.D., Kejariwal, A., Campbell, M.J., Mi, H., Diemer, K., Guo, N., Ladunga, I., Ulitsky-Lazareva, B., Muruganujan, A., Rabkin, S., et al. (2003). PANTHER: a browsable database of gene products organized by biological function, using curated protein family and subfamily classification. Nucleic Acids Res. *31*, 334–341.

Vasalauskaite, A., Morgan, J.E., and Sengpiel, F. (2019). Plasticity in adult mouse visual cortex following optic nerve injury. Cereb. Cortex *29*, 1767–1777. https://doi.org/10.1093/cercor/bhy347.

Vilcaes, A.A., Chanaday, N.L., and Kavalali, E.T. (2021). Interneuronal exchange and functional integration of synaptobrevin via extracellular vesicles. Neuron *109*, 971–983 e5. https://doi.org/10.1016/j.neuron.2021.01.007.

Wang, Y., Balaji, V., Kaniyappan, S., Kruger, L., Irsen, S., Tepper, K., Chandupatla, R., Maetzler, W., Schneider, A., Mandelkow, E., and Mandelkow, E.M. (2017). The release and trans-synaptic transmission of Tau via exosomes. Mol. Neurodegen. *12*, 5. https://doi.org/10.1186/s13024-016-0143-y.

Watanabe, T., Muranaka, N., Iijima, I., and Hohsaka, T. (2007). Position-specific incorporation of biotinylated non-natural amino acids into a protein in a cell-free translation system. Biochem. Biophys. Res. Commun. *361*, 794–799. https://doi.org/10.1016/j.bbrc.2007.07.099.

Wiesel, T.N., Hubel, D.H., and Lam, D.M. (1974). Autoradiographic demonstration of ocular-dominance columns in the monkey striate cortex by means of transneuronal transport. Brain Res. *79*, 273–279.

Xu, T., Park, S.K., Venable, J.D., Wohlschlegel, J.A., Diedrich, J.K., Cociorva, D., Lu, B., Liao, L., Hewel, J., Han, X., et al. (2015). ProLuCID: An improved SEQUEST-like algorithm with enhanced sensitivity and specificity. Journal of proteomics *129*, 16–24.

You, Y., Gupta, V.K., Graham, S.L., and Klistorner, A. (2012). Anterograde degeneration along the visual pathway after optic nerve injury. PLoS One *7*, e52061. https://doi.org/10.1371/journal.pone.0052061.

Yu, S., Li, X., Liu, G., Han, J., Zhang, C., Li, Y., Xu, S., Liu, C., Gao, Y., Yang, H., et al. (2007). Extensive nuclear localization of alpha-synuclein in normal rat brain neurons revealed by a novel monoclonal antibody. Neuroscience *145*, 539–555. https://doi.org/10.1016/j.neuroscience.2006.12.028.

Zhang, Z., Yu, W., Zheng, M., Liao, X., Wang, J., Yang, D., Lu, W., Wang, L., Zhang, S., Liu, H., et al. (2019). Pin1 inhibition potently suppresses gastric cancer growth and blocks PI3K/AKT and Wnt/beta-catenin oncogenic pathways. Mol. Carcinog. *58*, 1450–1464. https://doi.org/10.1002/mc.23027.

STAR★METHODS

KEY RESOURCES TABLE

REAGENT or RESOURCE	SOURCE	IDENTIFIER
Antibodies		
Goat anti-biotin	Thermo Fisher Scientific	Cat# 31852; RRID:AB_228243
Mouse anti-MAP2	Millipore	Cat# MAB3418; RRID:AB_11212326
Mouse anti-NeuN	Millipore	Cat# MAB377; RRID:AB_2298772
Mouse anti-Synaptotagmin	Millipore	Cat# MAB5200; RRID:AB_11213556
Mouse anti-Tau1	Sigma-Aldrich	Cat# T9450; RRID:AB_477595
Rabbit anti-Munc18	Sigma-Aldrich	Cat# M2694; RRID:AB_477176
Mouse anti-CaMKII	Novus	Cat# NB100-1983; RRID:AB_10001339
Goat anti-mouse HRP	Bio-Rad	Cat# 172-1011; RRID:AB_11125936
Goat anti-rabbit HRP	Bio-Rad	Cat# 172-1019; RRID:AB_11125143
Donkey anti-goat HRP	Bio-Rad	Cat# 172-1034; RRID:AB_11125144
Donkey anti-goat 488	Thermo Fisher Scientific	Cat# A-11055; RRID:AB_2534102
Donkey anti mouse 568	Molecular Probes	Cat# A-11004; RRID:AB_141371
Donkey anti-rabbit 568	Thermo Fisher Scientific	Cat# A10042; RRID:AB_2534017
Mouse anti-FLAG M2 antibody	Sigma-Aldrich	Cat#:F3165; RRID:AB_259529
Rabbit anti-Synuclein beta	Sigma-Aldrich	Cat# SAB4502827; RRID:AB_10761178
Mouse anti-Cre recombinase	Sigma-Aldrich	Cat# C7988; RRID:AB_439697)
Rabbit anti-GABA	Sigma-Aldrich	Cat# A2052; RRID:AB_477652)
Goat anti-Rabbit IgG: 15nm Gold	BBI Solutions	Cat# EM GAR15/1; RRID:AB_1769134
Rabbit anti Syntaxin 1	Gift Dr Anton Maximov	
Alexa Fluor 488 FluoroNanogold-Streptavidin	Nanoprobes	Cat# 7216; RRID:AB_2797136
Streptavidin Alexa 488	Thermo Fisher Scientific	Cat# S11223; RRID:AB_2336881
Bacterial and virus strains		
AAV-DJ	Gift from Dr Anton Maximov	N/A
Biological samples		
Healthy Rat fixed brain tissue.	Envigo (Harlan)	N/A
Healthy Rat dissected retinas, Optic nerve, LGN, SC and frontal cortex	Envigo (Harlan)	N/A
Xenopus, Transgenic Y2 line	National Xenopus Resource	RRID:SCR_013731
Chemicals, peptides, and recombinant proteins		
EZ-Link NHS-biotin (*N*-hydroxysuccinimidobiotin)	Thermo Fisher	Cat#20217
Critical commercial assays		
Fluorescence biotin quantitation kit	Thermo	Cat#46610
TSA Biotin system	Perkin Elmer	Cat#NEL700A001KT
ABC-HRP (Vectastain, elite)	Vector labs	Cat#LS-J1001-1
Goldenhance EM	Nanoprobes	Cat#2113
Pierce™ Monomeric Avidin Agarose	Thermo	Cat#20228
Pierce™ NeutrAvidin™ Agarose	Thermo	Cat#29201
Deposited data		
Proteomic data of NHS-biotin labeled samples from visual cortex	ProteomeXchange	ProteomeXchange: PXD030870

(*Continued on next page*)

Continued

REAGENT or RESOURCE	SOURCE	IDENTIFIER
Experimental models: Organisms/strains		
Rattus novergicus Strain (Sprague Dawley SD)	Envigo (Harlam)	IACUC protocol 08-0082
Mus musculus Ai9 strain line (B6.Cg-Gt(ROSA)26Sortm9(CAG-tdTomato)Hze/J)	Madisen et al., 2010.	IACUC protocol 08-0082
Xenopus laevis tadpoles (stage 47/48) with transgene expressing Cre reporter LCMV:ECFP(loxP)EYFP (Y2 line)	National Xenopus Resource Center, MBL	IACUC protocol 08-0083
Recombinant DNA		
pAAVII-Syn-Tau-3xFLAG	In house	N/A
pAAVII-Syn-SYNC-3xFLAG	In house	N/A
pAAVII-Syn-GFP-3xFLAG	In house	N/A
pAAVII-SYT-GFP-3xFLAG	In house	N/A
pAAVII-Stxbp1(Munc18)-GFP-3xFLAG	In house	N/A
pAAVII-Syn-GFP-CRE	Gift from Maximov lab	N/A
pAAVII-Syn-SNCB-CRE	In house	N/A
pCMV-synaptotagmin-TEV-Cre	In house	N/A
pCMV-Rop(Munc18)-TEV-Cre	In house	N/A
pCAG-Cre	Gift from Ruthazer lab	N/A
pCMV-synuclein-TEV-Cre	In house	N/A
Software and algorithms		
ImageJ	NIH	https://imagej.nih.gov/ij/
R version 4.0.0	R Foundation for Statistical Computing	N/A
Metamorph Version 7.10.1.161	Molecular Devices	N/A

RESOURCE AVAILABILITY

Lead contact

Further information and requests for resources and reagents should be directed to Hollis T. Cline (cline@scripps.edu).

Materials availability

This study did not generate unique reagents.

Data and code availability

Data: Proteomic data (raw unprocessed MS data files) have been deposited at ProteomExchange and are publicly available as of the date of publication, as described in the key resources table.

Code: This paper does not report original code.

Additional information required to reanalyze the data reported in this paper is available from the lead contact upon request.

EXPERIMENTAL MODEL AND SUBJECT DETAILS

All animal experiments were conducted in accordance with the guidelines of the Institutional Animal Care and Use Committee (IACUC) at the Scripps Research Institute (Protocol #08-0082 and #08-0083). Adult male rats were used for most experiments. For experiments in Xenopus, the tadpoles are too young for visual determination of sex and we assume approximately equal numbers of males and females were included in the study.

METHODS DETAILS

Intravitreal injection of NHS-biotin

Male Wistar rats (30-45 day old) were used for all *in vivo* intravitreal biotinylation procedures. Five milligrams of NHS-biotin (*N*-hydroxysuccinimidobiotin, EZ-Link® from ThermoFisher) were dissolved in 300 μl of sterile DMSO immediately before eye injection.

Intravitreal injections of 5 μl of solution were made in one or both eyes depending on the experiment by using a microinjector pressure system (Picosprizer II) with a manipulator attached to a pulled micropipette. The procedure was repeated 7 times, once a day over one week under deep anesthesia with (0.5 mg/kg Medetomidine and 75mg/kg ketamine ip). The eyes were treated with topical antibiotics and analgesics and examined daily. Control animals were injected following the same protocol with 5 μl of saline. The animals were euthanized 11-13 days after the first injection and were divided into different 2 groups: 1) For biochemistry, rats were euthanized with CO_2 and decapitated for brain removal. The tissue was frozen immediately in isopentane in dry ice and stored at −80°C. 2) For histology, animals were perfused with cold artificial cerebrospinal fluid (ACSF) and cold 4% PFA in 0.1 M phosphate buffer. Tissue was sliced using a vibratome (Leica) and stored in PBS with 0.02% sodium azide at 4°C for immunohistochemistry and immunofluorescence studies. For electron microscopy studies animals were perfused with cold ACSF then cold PFA 4% plus 0.1% glutaraldehyde.

Intravitreal injection of radiolabeled amino acids

Male Wistar rats (30-45 day old) were used. Groups of ten animals were injected in both eyes using the same procedures described above with 1 daily injection over 3 days with 5 μl solution containing a mix of 3.3 μCi/μl 35S-methionine and 1μCi/μl 3H-proline. Animals were sacrificed after 20 days. Brains and eyes were harvested and flash frozen in cold isopentane. For some experiments, 20 μm frozen sagittal sections were collected on Superfrost® plus microscope slides using a cryostat. For other experiments, dissected fresh tissue from retina, LGN, frontal and visual cortices were collected and homogenized in RIPA buffer. Radiolabeled proteins in the lysates were quantified using a liquid scintillation counter from PerkinElmer™ or loaded onto 4-20% SDS/PAGE gradient gel (Bio-Rad). Proteins were separated by electrophoresis and transferred to nitrocellulose membranes. Radiolabeled tissue sections and blotted nitrocellulose membranes were exposed to PhosphorImager screens or Kodak® BioMax® MR films inside autoradiography cassettes for 1 week and imaged by PhosphorImager or developed in an X ray film developer.

Histology in rodent brain sections

Selected brain sagittal sections containing LGN and optic tract were cut 40 μm thick using a vibratome (Leica VT1000S). The sections were quenched for 5 minutes and blocked for 1 h with 3% normal donkey serum and 0.3% Tween 20 in PBS. The sections were then incubated overnight at 4°C with the following primary antibodies (1:500 Goat anti-biotin, Pierce, 1:200 mouse anti-MAP2, Chemicon, 1:2000 mouse anti-Flag, Sigma or 1:200 mouse anti-NeuN, Millipore). After three washes in PBS/0.3% Tween 20, the sections were incubated in a 1:200 dilution of the following secondary antibodies (anti-goat alexa 488 and anti-mouse alexa564, Invitrogen) for 1 hour at room temperature in blocking buffer. The stained sections were mounted in Vectashield mounting medium (Vector lab) and images were obtained using a Spinning disc confocal (Ultraview VOX, Perkin Elmer) or laser scanning confocal (Olympus FV500) microscope.

Electron microscopy

Detection of biotinylated proteins in the retinogeniculate pathway: Selected sagittal and coronal sections were cut at 50 μm thick with a vibratome. Slices were then quenched with 100mM glycine in PBS for 2 h and endogenous peroxidase activity was blocked with 0.5% of H_2O_2 and 1% normal goat serum (NGS) in PBS for ½ hour. Sections were blocked with 10% NGS in PBS for 1 h and incubated overnight with ABC reagent (1 drop of A and 1 drop of B in 5 ml PBS with 1% NGS, Vector Lab). Signal was amplified using a tyramide amplification system (TSA kit from Perkin Elmer) and detected by diaminobenzidine (DAB) reagent (SigmaFast™) with nickel enhancement. In some sections, biotinylated proteins were labeled by overnight incubation with 1:100 streptavidin-FluoroNanogold particles 1.4 nm size (Nanoprobes) in 1% NGS and 0.001% Triton x (Roche), post fixed for 20 min in Karnovsky fixative, containing 4% paraformaldehyde, 5% glutaraldehyde in PBS, and enhanced for visualization with Goldenhance kit (Nanoprobes) as described (Schikorski, 2010).

Detection of Flag labeled proteins in the retinogeniculate pathway: Brain sections expressing Flag labeled TNTPs were quenched with glycine, H_2O_2, blocked as mentioned above and incubated with 1:2000 mouse anti-Flag antibody overnight (clone M2, Sigma). After three washes in PBS, sections were incubated with 1:200 goat biotinylated anti-mouse antibody (DSB-X Biotin, Invitrogen) in blocking buffer for 2 h at room temperature. Sections were washed 3 times in PBS and incubated with ABC reagent and stained with DAB as mentioned above but without tyramide amplification. Right after DAB staining, sections that contained labeled retinogeniculate axons were then post fixed with 1% OsO_4 in PBS for ½ h, dehydrated with an ethanol series (50%, 70% with 4% uranyl acetate, 90%, 100%), washed 3 times with pure acetone and flat embedded in resin (Embed-812, Electron Microscopy Sciences) between two sheets of Aclar plastic (Electron Microscopy Sciences) and polymerized in a vacuum oven at 60°C overnight.

Selected sections that contain biotin labeled terminals were cut into 50-60nm ultrathin sections using a diamond knife (Diatome, Switzerland) on an ultramicrotome (Powertome XL, RMC products). Ultrathin sections were mounted on 2 × 1 mm nickel slot grids (Ted Pella) coated with piloform film. Every 20th section was collected to avoid oversampling the same terminal. In some experiments (Figure 3), serial sections were collected and used for postembedding immunostaining for GABA following previously reported immunocytochemical protocols (Li et al., 2003). We used a rabbit polyclonal antibody against GABA (Sigma) at a dilution of 1:500 and a goat-anti-rabbit IgG conjugated to 15 nm gold particles (British BioCell International). The GABA-immunolabeled sections were air-dried and stained with a 10% solution of uranyl acetate in methanol for 20 minutes, washed 3 times in methanol and dried before examination under the electron microscope. The criteria to distinguish GABA positive profile was that the density of gold particles

was higher than that found in 95% of the surrounding corticothalamic terminals that had round synaptic vesicles, small profile, and asymmetric synaptic contacts. Corticothalamic terminals are exclusively non-GABAergic (Montero and Singer, 1985; Beaulieu and Cynader, 1992). We found that all GABAergic profiles postsynaptic to retinogeniculate terminals had synaptic vesicles inside, independent of the synaptic contacts they made, consistent with previous studies (Li et al., 2003). We therefore used the criteria of presence or absence of synaptic vesicles to distinguish GABAergic postsynaptic and non-GABAergic profiles of retinogeniculate terminals, respectively.

Quantification of labeled protein transfer in electron microscopy images

ROIs were drawn around postsynaptic profiles apposed to labeled (labeled-apposed; marked as "a" in a schematic in Figures 2G and 6B) or unlabeled (unlabeled-apposed; marked "b" in schematic in Figures 2G and 6B) presynaptic profiles on 16-bit greyscale electron microscopy (EM) images. The pixel intensity values from each ROI were detected with ImageJ, logged and binned as counts into 256 equal bins of intensity ranging from 0 to 65535 to generate a pixel intensity histogram from each ROI. Each histogram bin was normalized to total pixels in the ROI (area) to obtain a normalized pixel intensity histogram. For each image, all labeled-apposed and unlabeled-apposed normalized pixel intensity histograms were averaged separately and a bin ratio histogram of labeled-apposed ROI/unlabeled-apposed ROI was obtained. The bin ratio histogram normalizes the pixel intensity distribution of labeled-apposed postsynaptic profiles over the background pixel intensity distribution of unlabeled-apposed postsynaptic profiles from the same image. The bin ratios would be 1 when intensity distribution of labeled-apposed and unlabeled-apposed ROIs is equal, and higher than 1 in bins where labeled-apposed ROIs show higher pixel intensity counts compared to unlabeled-apposed ROIs. The ratio histograms from each image were generated (Figure S6H) aligned by the peak ratio, using the bin that displayed the maximum ratio, to obtain an average ratio histogram from all data. For final graphic display, 256 bins were trimmed to 64 bins surrounding maxima of the average peak. For statistics, P-value was calculated by comparing ratio histograms of labeled- and control samples using two-way ANOVA with Sidak correction for multiple comparisons.

Purification of biotinylated proteins from rat brain

Tissue samples from 10 to 12 brains were pooled for total protein extraction. Lateral geniculate nucleus, visual and frontal cortices were dissected from fresh brain and homogenized in cold lysis buffer containing 150 mM NaCl, 50mM TrisHCl pH = 7.4, 1%NP40, 0.5 % sodium deoxycholate, 0.1% SDS and protease inhibitor Cocktail (Complete® from Roche). The protein homogenates were briefly sonicated, rotated for 1 h at 4°C and centrifuged for 15 min at 10,000g at 4°C. Supernatants were collected, protein concentration was measured by DC Protein Assay kit® (Bio-Rad), and samples were used for biotinylated protein purification or immunoprecipitation of candidate MS/MS hits. For biotinylated protein purification, 40-50 milligrams of protein extract (from visual and frontal cortex samples) or 2-4 mg (from LGN) were loaded onto chromatographic columns packed with 2ml monomeric avidin resin (Pierce). The columns were then washed with 10 column volumes of PBS making sure that protein content was absent in the last flow through washes. The bound biotinylated proteins where eluted from the column by competition with 3mM of biotin in PBS and eluted samples were then dialyzed to remove free biotin and concentrated using Amicon Ultra® concentrator tubes (Millipore) (Data in Figure 1).

For immunoprecipitation of TNTPs from cortex (Data in Figure 4), five milligrams of protein extract from either visual or frontal cortex was incubated for 2 h at room temperature with 400 μl of antibody coupling resin (aminoLink®, Pierce Co-Immunoprecipitation kit) conjugated to rabbit anti-Munc18, rabbit anti-Syntaxin 1A or mouse anti-CaMKII (Chemicon). The resin was washed 5 times with PBS containing 0.3% Triton X100. Washes of resin were done until no protein was detected in the flow through by measuring absorbance at 280nm with a Nanodrop spectrophotometer (Thermo scientific). The elution of the immunocomplexes was done by mixing the resin with 100 μl of a low pH elution buffer from the kit (pH=2.8). Immunopurified protein was then neutralized by adding 10 μl of 1M Tris pH=9.5 before western blotting. In some experiments the immunocomplexes were further incubated with Neutravidin beads for enriching biotin-labeled protein from the total immunopurified proteins. In this case the immunopurifed proteins were diluted to 1 ml in RIPA buffer and then incubated with 50 μl of Neutravidin beads (Thermo) for 1 hour at room temperature. The beads were then washed 3 times in RIPA buffer and eluted in Laemmli sample buffer and used for western blot analysis.

Western blots

Eluates containing purified biotinylated protein were loaded onto 4-20% SDS/PAGE gradient gel (Bio-Rad). In experiments with immunoprecipitates, the samples were loaded onto 8% SDS/PAGE gels. Proteins were separated by electrophoresis, transferred to nitrocellulose membranes (Bio-Rad) and incubated for 1 hour in blocking buffer containing 0.05 % Tween 20, 20 mM Tris.HCl, 133 mM NaCl, pH:7.4 (TBST) and 5% non-fat milk (Bio-Rad). The membranes were then incubated in blocking buffer for 24 hours with the following antibodies: goat anti-biotin antibody 1:1000 (Thermo) for detecting biotinylated bands; 1:1000 mouse anti-Munc18 from Sigma; 1:1000 mouse anti-CaMKII from Novus; 1:500 rabbit anti-Tau or 1:1000 rabbit anti-Syntaxin 1A (gift from Dr. Anton Maximov). Membranes were washed 3 times for 10 min in TBST and incubated in blocking buffer at room temperature for 1 h with a 1:2500 dilution of: anti-mouse, anti-rabbit or anti-goat secondary antibodies conjugated with HRP (Bio-Rad). Bands were detected by chemiluminescence using ECL western blotting substrate® (Figures 1 and 5) or SuperSignal West femto® (Pierce) and Kodak Biomax XAR films (Figure 4). Quantification of optical densities of the bands was made using ImageJ software.

Tissue and protein sample processing for mass spectrometry

Tissue samples were collected from animals with intravitreal injections of NHS-biotin or saline following treatment protocols described above. We used two independent experimental approaches for sample preparation, one using standard monomeric avidin protein enrichment followed by protein digestion, and the other, called DiDBiT for direct detection of biotin tag, using protein digestion followed by Neutravidin purification of biotinylated peptides, which eliminates the problem of contaminating non-biotinylated proteins seen in the Neutravidin protein enrichment strategy, as described in our previous studies (Liu et al., 2018; Schiapparelli et al., 2014, 2019).

For the protein enrichment strategy, 5 independent experiments were conducted in which tissue was collected from 2 groups of 10 to 12 animals/group for each experiment. Tissue samples from the 10 to12 brains/group were pooled for total protein extraction. Visual cortices were dissected from fresh brain and homogenized in cold lysis buffer containing 150 mM NaCl, 50mM TrisHCl pH=7.4, 1%NP40, 0.5 % sodium deoxycholate, 0.1% SDS and protease inhibitor Cocktail (Complete® from Roche). The protein homogenates were briefly sonicated, rotated for 1 h at 4°C and centrifuged for 15 min at 10,000g at 4°C. Supernatants were collected, protein concentration was measured and 40-50 milligrams of protein extract from visual cortex were loaded onto chromatographic columns packed with 2ml monomeric avidin resin (Pierce). The columns were then washed with 10 column volumes of PBS. The bound biotinylated proteins where eluted from the column by competition with 3mM of biotin in PBS and eluted samples were then dialyzed to remove free biotin and concentrated using Amicon Ultra® concentrator tubes (from Millipore).

For the DiDBiT strategy for direct identification of biotin modified proteins in LGN and visual cortex we followed the protocol as we previously described (Schiapparelli et al., 2014, 2019). Two independent experiments were conducted in which tissue was collected from 2 groups of 10 to 12 animals/group injected with NHS-biotin or saline. Tissue from each group was pooled, then homogenized in RIPA buffer as described above. Protein was quantified and precipitated by adding 3 volumes of methanol, 1 volume of chloroform and 3 volumes of water, vortexed and centrifuged at 15,000 g for 2 min at room temperature. The aqueous and organic phases were carefully removed from the tube without disturbing the protein disc at the interface. Protein pellets were washed once by adding 3 volumes of methanol and centrifuging at 15,000 g for 2 min. Pellets containing biotinylated proteins were air dried for 10 min before total protein digestion as follows. Protein pellets were digested with trypsin and ProteaseMax surfactant trypsin enhancer (Promega) in all experiments following the DiDBiT strategy, except where indicated below. We resuspended the protein pellet in 200 μl of buffer containing 4 M urea, 50 mM NH_4HCO_3 and 0.1 % ProteaseMax with a brief sonication pulse. The protein suspension was reduced by adding 5 mM Tris(2-carboxyethyl)phosphine (TCEP, Sigma). The solution was incubated at 55°C with vigorous orbital shaking using a Thermomixer (Eppendorf). Protein alkylation was done by adding 10 mM iodoacetamide (Sigma) and incubating with vigorous shaking in the dark for 20 min. To digest the proteins, we added in the following order: 150 μl of 50 mM NH_4HCO_3, 2.5 μl of 1 % ProteaseMAX dissolved in 50 mM NH_4HCO_3 and 1:100 (enzyme/protein, w/w) sequencing grade trypsin (Promega) to a final reaction volume of 500 μl. The digestion reactions were incubated for 3 h at 37°C with vigorous orbital shaking and stored at −80°C until enrichment of biotinylated peptides. The digestion reactions were stopped by adding 0.1% trifluoroacetic acid, TFA (Sigma). Samples were centrifuged at 20,000g for 20 min at room temperature to remove undigested insoluble material and supernatant containing the peptide mixture was collected in an Eppendorf tube. Any remaining peptides in the insoluble pellet were extracted by adding 0.5 ml of 0.1% TFA, resuspending the pellet by pipetting and centrifuging again for 20 min. The supernatant was pooled with the previous one before desalting using Sep-Pak tC18 solid-phased extraction cartridges (from Waters). Prior to loading the mixture of peptides, the cartridges were washed sequentially with 3 ml of acetonitrile, 3 ml of 0.5% acetic acid, 50% acetonitrile in water, and with 3 ml of 0.1% TFA in water. After loading the peptide mixtures, the cartridges were washed with 3 ml of 0.1% TFA and then with 0.250 ml of 0.5% acetic acid in water. The peptides were eluted into a clean tube with 1 ml of 0.5% acetic acid, 80% acetonitrile in water and dried in Eppendorf tubes in a Speed Vac (Thermo). Ten milligrams of dried peptide pellet were solubilized in 1 ml of PBS and incubated with a 200 μl slurry of Neutravidin beads (Pierce) for 1 h at room temperature. The beads were precipitated by centrifugation at 1000 g for 5 min and flow through was collected for MS analysis of unbound peptides. Beads were washed 3 times by adding 1 ml of PBS, 3 times with 1 ml of 5% acetonitrile in PBS and with a last wash in ultrapure water. Excess liquid was completely removed from the beads using a micropipette and biotinylated peptides were eluted by adding 0.3 ml of solution containing 0.2% TFA, 0.1% formic acid, 80% acetonitrile in water. The beads were centrifuged at 1000 g and the first elution of biotinylated peptides was transferred to an Eppendorf tube. A second elution of 0.3 ml was boiled for 5 min for maximum release of peptides from the beads. A total of 10 elutions were collected and dried separately in a Speed Vac. The enriched biotinylated peptides were resuspended in 0.2 ml PBS and the pH was corrected by adding 20 μl of 1.5 M TrisHCl buffer (pH=7.4). A 10 μl aliquot of the elution was taken to measure biotinylated peptide content.

Protein identification by LC-MS/MS

Digested proteins, prepared as mentioned above in the PE protocol, or purified biotin-tagged peptides from the DiDBiT protocol were pressure-loaded onto a 250-μm i.d capillary with a kasil frit containing 2 cm of 10 μm Jupiter C18-A material (Phenomenex) followed by 2 cm 5 μm Partisphere strong cation exchanger (Whatman). This column was washed with Buffer A (95% water, 5% acetonitrile, 0.1% formic acid) after loading. A 100 μm i.d capillary with a 5 μm pulled tip packed with 15 cm 4 μm Jupiter C_{18} material (Phenomenex) was attached to the loading column with a union and the entire split-column (loading

column–union–analytical column) was placed in line with an Agilent 1100 quaternary HPLC (Palo Alto). The DidBiT samples were analyzed using a modified 1 to 8-step MudPIT separation described previously (Schiapparelli et al., 2019). As peptides eluted from the microcapillary column, they were electrosprayed directly into a Velos mass spectrometer (ThermoFisher) with the application of a distal 2.4 kV spray voltage. A cycle of one full-scan FT mass spectrum (300-2,000 m/z) at 60,000 resolution followed by 20 data-dependent IT MS/MS spectra at a 35% normalized collision energy was repeated continuously throughout each step of the multidimensional separation. Exosomes samples were eluted on a column self-packed with BEH (Ethylene BridgedHybrid) (Waters 100 μm inner diameter × 1.7 μm × 20 mm) using a 1–30% gradient of solvent B for 160 min, 30–90% for 60 min, and 90% for 20 min at a 200 μL/minflow rate using a Easy-1000 UPLC coupled to an Orbitrap Lumos Tribid (Thermo Fisher). The Orbitrap Lumos was operated in data-dependent acquisition mode using the Multinotch MS3 method through the XCalibur software. Survey scan mass spectra were acquired in a positive ion mode in the 400–1500 m/zrange with the resolution set to 120,000 (fwhm; full width half maximum) and AGC target of 4×10^5 on the Orbitrap. The ten most intense ions per survey scan containing 2–7charges were selected for CID fragmentation, and the resulting fragments (MS2) were analyzed in the ion trap in the 400–120 m/z range. Dynamic exclusion was employed within 10 s to prevent repetitive selection of the same peptide. The ten most intense MS2 fragments were selected for HCD fragmentation (MS3), and the resulting fragments were detected in the Orbitrap in the 120–500 m/zrange with the resolution set to 15,000 (fwhm) and AGC target of 10^5.

Processing mass spectra and protein identification

MS/MS spectra were searched with the Prolucid algorithm (Xu et al., 2015) against the Uniprot rat database (Release date 3.25.14) concatenated to a decoy database in which the sequence for each entry in the original database was reversed. Mass shifts of 229.1629 on lysine/N-terminus (TMT exosomes) and 57.02146 on cysteine (all samples) were searched as static modifications. Differential modification of lysine residue as the result of EZ-Link NHS-Biotin linking reaction was set as 226.0776. The search results were assembled and filtered using the DTASelect 2.0 program (Lavallee-Adam et al., 2015). Peptides were required to be partially tryptic, less than 10ppm deviation from peptide match, and an FDR at the protein level of 0.01.

Proteome analysis

Distribution of TNTPs according to their cellular localization was curated manually using open source databases of subcellular localization of proteins (Pielot et al., 2012; Thomas et al., 2003). Gene ontology analysis of the synaptic compartment was done using SYNGO databases (Koopmans et al., 2019). Gene ontology of molecular function analysis was done using http://pantherdb.org database (Mi et al., 2019). Enrichment of presynaptic proteins analysis in TNTPs list was done using SynaptomeDB databases (Pirooznia et al., 2012) comparing enrichment in RGC transportome databases from our previous study (Schiapparelli et al., 2019) using Fisher's exact test. The scheme of the TNTPs and their roles in axonal and synaptic compartments is based on the KEEG database (Kanehisa, 2000). We conducted bioinformatic analysis of the TNTP dataset using the COMPARTMENTS platform (https://compartments.jensenlab.org) for subcellular localization or Gene Ontology with cellular components complete (geneontology.org) (Ashburner et al., 2000; Binder et al., 2014; The Gene Ontology, 2019) show that extracellular vesicles are prominent in the top 10 subcellular localization categories ranked by highest significance. Network analysis using the STRING databases (Szklarczyk et al., 2017) with links representing known interactions with high level of confidence (0.7).

Analysis of TNTP release and packaging into exosomes

To test whether TNTPs are released from neuronal exosomes, rat cortical primary neurons were infected with AAV-DJ expressing TNTP-FLAGs: β-synuclein, synaptotagmin 1, tau or Munc18, and the exosome markers, alix- and flotilin-FLAG. Conditioned media was collected over a 2-day period and exosomes were purified as described. TNTP-FLAG packaging and release from neurons was assessed by comparing FLAG signal in exosomes and neurons.

In vivo analysis of TNTP transfer in rats

Adult 2 month old rats were administered AAV-DJ using intravitreal injection as described above for NHS-biotin. AAV-DJ viral expression vectors were produced using a shuttle vector with the WPRE element and the hGH polyadenylation signal flanking the encoding sequence (Cardin et al., 2010), generous gift from the Maximov lab). Expression of Flag tagged on C-terminals fusion construct was driven by a 1.1Kb rat Synapsin promoter. The Flag tagged versions of β-synuclein, Munc18, synaptotagmin-1, alix and GFP were detected in coronal sections of LGN using a mouse anti-Flag M2 monoclonal antibody (Sigma). Two-four weeks after injection, animals were intracardially perfused and brain tissue was processed as described above for light and immunoelectron microscopy detection of Flag labeled proteins. Our observation that GFP-FLAG is not detected in postsynaptic profiles after intravitreal viral infection indicates that intravitreal injections of the AAV-DJ serotype do not result in direct infection of LGN neurons or anterograde transfer of virus. For analysis shown in Figure 7, we measured FLAG pixel intensity (green) in MAP2+ (red) cell bodies in the labeled ipsilateral LGN projection domain and normalized these values to signal in the unlabeled control contralateral domain in the same images of LGN [regions 2 and 3 in (Figure 7A)].

For analysis in Figure S8, we used Ai9 mice line (B6.Cg-Gt(ROSA)$^{26Sortm9(CAG-tdTomato)Hze/J}$ (Madisen et al., 2010) that induces expression of the reporter tdTomato upon the expression of cre recombinase. AAV-DJ expressing synuclein-cre recombinase fusion

protein was injected intravitreally into 3 month-old Ai9 mice anesthetized with ketamine/xylazine. To prepare retinal sections, the tissue was cryoprotected by incubating the eyes 3 days in 30% sucrose in 0.1M PB at 4°C and embedded in OTC compound. Retinal sections were cut at 30 μm thick using a cryostat (Leica CM3050S). Retina sections were examined to confirm successful transduction of retinal cells including RGCs. Different serotypes of AAVs were tested to achieve the highest transduction efficiency. For the final experiments, we used AAV-DJ serotype, which is a fusion of multiple serotypes (Grimm et al., 2008) that yielded the highest transduction efficiency in mice retina.

Histology

To evaluate GFP and tdTomato expression in Ai9 mice, animals were sacrificed 1-6 months after retinal injection, perfused with 4% PFA in PBS and the brains were dissected and post fixed in 4% PFA at 4C overnight. Sagittal or coronal brain sections (50-100 μm) were cut on the vibratome and mounted in clearing reagent (6M urea in 50% glycerol) with DAPI or Hoechst added. Sections were imaged on Nikon C2 confocal microscope with 10/20x air objectives and digital montages were made with Nikon Elements acquisition software.

Analysis of TNTP transfer in primary neuronal culture

To test whether TNTP-cre recombinase fusion proteins are transferred between mammalian neurons, we screened for TNTP transfer in co-cultures of Ai9 transgenic cortical neurons that express floxed tdTomato with wild type cortical neurons transfected in suspension (nucleofection) with TNTP-cre recombinase and floxed GFP using Amaxa mouse neuron Nucleofector kit and Nucleofector II device (Lonza) according to the manufacturer's instructions. After washing extensively in plating medium containing Neurobasal-A medium, B27 supplement, 2 mM L-glutamine (Gibco) and 2.5 % Fetal bovine serum (Hyclone), 100,000 nucleofected wild type neurons were mixed with an equal number of Ai9 transgenic neurons and plated in 12 well plates in plating media. Media was replaced 3 h after plating with medium containing Neurobasal-A, B-27 supplement, 2 mM L-glutamine. Over 3-5 weeks *in vitro*, we screened for tdTomato expressing neurons in co-cultures expressing synuclein-cre recombinase or control-cre recombinase.

In Vivo analysis of TNTP-Cre recombinase transfer in Xenopus laevis tadpoles

DNA constructs and electroporation: Sequences encoding TNTPs were fused at the N- or C-terminals to cre-recombinase and subcloned into expression vectors under the CMV promoter. Stage 46 transgenic tadpoles expressing cre reporter LCMV:ECFP(loxP) EYFP (Y2 line, National Xenopus Resource Center, MBL) were electroporated unilaterally in the right tectum with TNTP-cre recombinase expressing DNA constructs. The transgenic tadpoles expressed CFP throughout the brain in the absence of cre-recombinase. Upon transfection, the cre recombinase fusion protein recombines the loxP sites and switches the CFP expression to YFP in the transfected cell. Unilateral electroporation was achieved using a large size electrode with the metal blades covering the length of the tadpole brain from forebrain to hindbrain and electroporation was done with unipolar current. Pilot experiments with GFP-expressing constructs were conducted to ensure that only cells on the electroporated side would be transfected. The protocol for electroporation had been described in detail previously (Haas et al., 2002).

Histology

For immunohistochemistry of tadpoles, animals were anesthetized in 0.02% MS222, and *in vivo* images were collected with a Nikon C2 confocal microscope equipped with 10/20x air objectives and then animals were fixed in 4%PFA at 4C overnight. Vibratome sections (40 μm thick) were prepared for free floating immunostaining. Sections were quenched in 1% $NaBH_4$ in PBS for 15min, then blocked in 10% normal goat serum in PBS with 0.5% triton for 1hr at room temperature. Sections were then incubated in mouse monoclonal Cre recombinase antibody (Sigma, C7988) at a 1:1000 dilution in 1% serum in PBS with 0.5% triton at 4C overnight followed by 1 hour incubation in Alexa488 goat anti- mouse secondary antibody (1:500, Invitrogen, CA) at room temperature.

In vivo imaging and data analysis: Tadpoles were examined 2-3 days after electroporation for the expression of YFP in the electroporated side (right) of brain. Animals with low transfection rate on the right side of the brain or animals with any visible YFP expression on the un-electroporated side were excluded from experiments. On 11∼13 days after electroporation, animals were anesthetized in 0.02% MS222 and imaged using an Ultraview VoX confocal system and Volocity 5 image acquisition software (Perkin-Elmer, Foster City, CA) with a XLUMPLFL 20 (0.9 NA) objective (Olympus), as described (Bestman et al., 2012). The left and right tectal lobes, forebrain, and hindbrain were imaged from the dorsal surface to 80∼100μm depth with 1μm z-step. CFP and YFP signals were excited with 405- and 488-nm lasers and emissions were collected with the 485(60) and 587(125) nm filters sequentially. This acquisition setting was not optimal for CFP excitation but ensured minimal YFP excitation in the CFP channel. The image stacks were analyzed in Volocity. For all experimental groups, single cells were identified in the YFP channel using an automatic object recognition algorithm with the same morphological criteria and intensity threshold. The ratio of YFP/CFP within each soma was calculated. Non-electroporated transgenic control animals (Tg control) from the same batch were used to evaluate the background level of YFP/CFP. For transgenic control animals, cells were identified in the CFP channel due to the low level of YFP signal. The YFP/CFP values within the Tg control group were very consistent from animal to animal and the mean + 2SD of the Tg control was used as the threshold for YFP-positive cells. The number of positive YFP cells on

the non-electroporated contralateral side (left) of brain was then counted for each animal. All images were also visually examined to exclude cell shaped smudges and artifacts. All of the image acquisition and analysis parameters were kept constant across all experimental groups.

STATISTICAL ANALYSES

We used JMP and PRISM for quantitative analyses of data, including the use of parametric and nonparametric tests depending on the data distribution and experimental design and testing for outliers in datasets that had been transformed with BoxCox. Experiments designed to compare VC vs FC or pairs of experimental and control conditions were analyzed used the Student's t test, Mann Whitney and Welsh's t test, depending on the distribution and variance of the datasets. Analyses of with multiple comparisons used ANOVA with correction for multiple comparisons. Samples sizes were based on power studies from initial or comparable data sets. A table of the data structure and type of statistical test used is in supplemental information. Sample sizes, N values, statistical tests, p values are in the figure legends.